Article

Molecular Cell

Enhanced Bacterial Immunity and Mammalian Genome Editing via RNA-Polymerase-Mediated Dislodging of Cas9 from Double-Strand DNA Breaks

Graphical Abstract

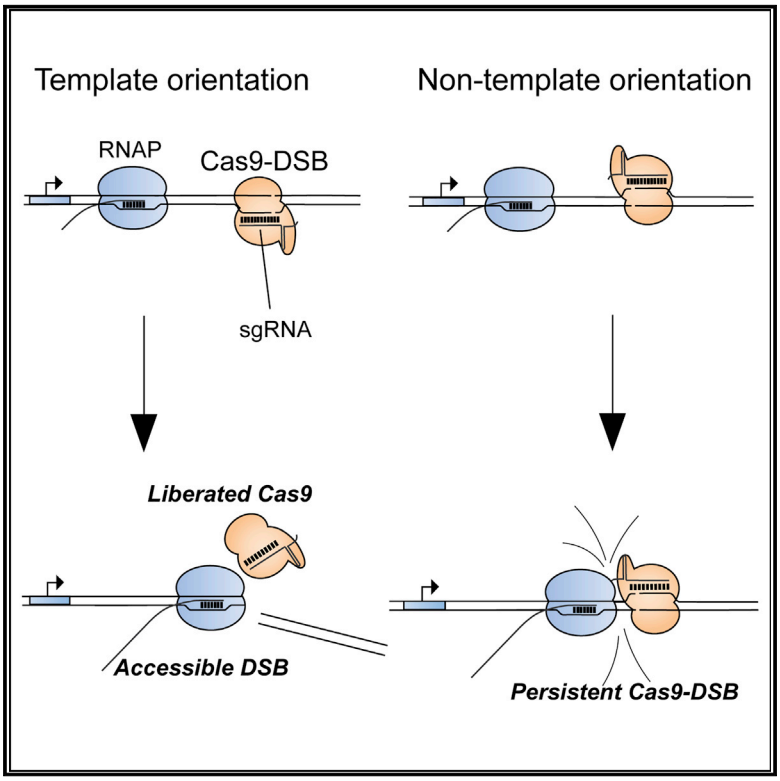

Authors

Ryan Clarke, Robert Heler, Matthew S. MacDougall, ..., George M. Church, Luciano A. Marraffini, Bradley J. Merrill

Correspondence

merrillb@uic.edu

In Brief

Clarke et al. show that persistent Cas9 binding to double-strand DNA breaks (DSBs) blocks DNA break repair. The Cas9-DSB complex can be disrupted by translocating RNA polymerases in a strand-biased manner, increasing genome editing frequencies and enhancing bacterial immunity to phages through multi-turnover Cas9 cleavage of phage genomes.

Highlights

- Persistent Cas9 binding blocks DNA repair proteins from accessing Cas9-generated breaks
- RNA polymerase can dislodge Cas9 from DNA breaks in a highly strand-biased manner
- Dislodging Cas9 with RNA polymerase generates multi-turnover nuclease activity
- Targeting of Cas9 to phage genome is strand biased toward multi-turnover activities

Clarke et al., 2018, Molecular Cell *71*, 42–55
July 5, 2018
https://doi.org/10.1016/j.molcel.2018.06.005

CellPress

CellPress

Molecular Cell
Article

Enhanced Bacterial Immunity and Mammalian Genome Editing via RNA-Polymerase-Mediated Dislodging of Cas9 from Double-Strand DNA Breaks

Ryan Clarke,[1] Robert Heler,[2] Matthew S. MacDougall,[1] Nan Cher Yeo,[3] Alejandro Chavez,[3] Maureen Regan,[1,4] Leslyn Hanakahi,[5] George M. Church,[3] Luciano A. Marraffini,[2] and Bradley J. Merrill[1,4,6,*]

[1]Department of Biochemistry and Molecular Genetics, University of Illinois at Chicago, Chicago, IL 60607, USA
[2]Laboratory of Bacteriology, The Rockefeller University, New York, NY 10065, USA
[3]Department of Genetics, Harvard Medical School, Wyss Institute for Biologically Inspired Engineering, Harvard University, Boston, MA 02115, USA
[4]Genome Editing Core, University of Illinois at Chicago, Chicago, IL 60607, USA
[5]Department of Medicinal Chemistry and Pharmacognosy, College of Pharmacy, University of Illinois at Chicago, Rockford Health Science Campus, Rockford, IL 61107, USA
[6]Lead Contact
*Correspondence: merrillb@uic.edu
https://doi.org/10.1016/j.molcel.2018.06.005

SUMMARY

The ability to target the Cas9 nuclease to DNA sequences via Watson-Crick base pairing with a single guide RNA (sgRNA) has provided a dynamic tool for genome editing and an essential component of adaptive immune systems in bacteria. After generating a double-stranded break (DSB), Cas9 remains stably bound to DNA. Here, we show persistent Cas9 binding blocks access to the DSB by repair enzymes, reducing genome editing efficiency. Cas9 can be dislodged by translocating RNA polymerases, but only if the polymerase approaches from one direction toward the Cas9-DSB complex. By exploiting these RNA-polymerase/Cas9 interactions, Cas9 can be conditionally converted into a multi-turnover nuclease, mediating increased mutagenesis frequencies in mammalian cells and enhancing bacterial immunity to bacteriophages. These consequences of a stable Cas9-DSB complex provide insights into the evolution of protospacer adjacent motif (PAM) sequences and a simple method of improving selection of highly active sgRNAs for genome editing.

INTRODUCTION

The clustered regularly interspaced short palindromic repeats (CRISPR) system provides bacteria and archaebacteria an adaptive immune system (Barrangou and Marraffini, 2014). In type II CRISPR systems, immunity begins during the adaptation phase wherein foreign DNA elements near the system's protospacer adjacent motif (PAM) sequence are recognized and then processed and inserted as the spacers into the CRISPR locus (Barrangou et al., 2007; Garneau et al., 2010; Heler et al., 2015). The immunization phase then begins through expression of the CRISPR loci and is characterized by spacer transcripts being processed into crRNA (Deltcheva et al., 2011). crRNAs direct Cas9 nuclease activity to foreign DNA by forming a ribonucleoprotein complex with Cas9 and tracrRNA and using the crRNA sequence to identify targets (Jinek et al., 2012). The PAM is an important component that prevents Cas9 from cutting the spacer sequence in its own genome by enabling nuclease activity only when the crRNA target sequence is adjacent to the short DNA sequence also used during the capture of spacers from the foreign DNA (Heler et al., 2015). For repurposing Cas9 to edit gigabase-sized genomes, Watson-Crick base pairing of the 5′ 20 bp of a single guide RNA (sgRNA) has provided sufficient specificity for widespread use of *Streptococcus pyogenes* Cas9 (spCas9) in editing various genomes, including those of mammals (Hsu et al., 2013; Jinek et al., 2013; Mali et al., 2013).

The basic biochemical and biophysical characteristics of spCas9 have been elucidated and exploited for genome editing. The ability to target a single site within the genome without off-target effects has been the focus of considerable research effort (Chen et al., 2017; Kleinstiver et al., 2016; Slaymaker et al., 2016). The relatively minor restrictions the PAM places on genomic sites that can be targeted and the ease of targeting Cas9 by expressing a short sgRNA have combined to support widespread and pervasive use of Cas9 for genome editing (Barrangou and Doudna, 2016).

In addition to the biochemical properties of Cas9 that provide its target specificity, the nuclease displays other unique properties that distinguish it from non-RNA-guided effector nucleases of bacterial immune systems, such as restriction endonucleases. In contrast to other endonucleases, Cas9 exhibits a remarkably stable enzyme-product state wherein the nuclease remains bound to the double-stranded break (DSB) it generates (Jinek et al., 2014; Nishimasu et al., 2014; Richardson et al., 2016). The Cas9-DSB state has been shown to persist *in vitro* for ~5.5 hr (Richardson et al., 2016). Nuclease dead Cas9 (dCas9)

and active Cas9 display the same slow off-rate *in vitro* (Richardson et al., 2016). Recent characterization of dCas9 in *Escherichia coli* reported stable binding to target DNA until DNA replication occurs (Jones et al., 2017). Although persistence of Cas9 binding for hour-long periods has not been examined in mammalian cells, fluorescence recovery after photobleaching and single-molecule fluorescence studies demonstrated persistence of dCas9 binding during minute-long observations (Knight et al., 2015). Thus, the slow off-rate appears to affect Cas9 functionality *in vitro* and *in vivo*.

In contrast to the rapid characterization for how Cas9 targets DNA, the consequences of the persistent enzyme-product state are not understood. The single-turnover characteristic could limit Cas9's effectiveness when DNA substrates are abundant, such as during phage infection. When DNA substrates are rare, such as when Cas9 is used to edit a unique mammalian genomic sequence, persistence of Cas9-DSB could preclude repair of the DSB by the cell. To date, experimental techniques to manipulate the kinetics of Cas9 dissociation from the DSB have been limited, which has prevented direct analysis of the consequences of the highly stable enzyme-product complex.

In this study, we show that the Cas9-DSB complex can be disrupted by RNA polymerase transcription activity through the Cas9 target site, but only if the sgRNA of Cas9 is annealed to the DNA strand used as the template by the RNA polymerase. The profound difference caused by the direction of the translocating RNA polymerase enabled examination of the effects of the persistent Cas9-DSB state. Dislodging Cas9 from the DSB stimulates editing efficiency in cells by allowing the ends of the DSB to be accessed by DNA repair machinery. This mechanism causes sgRNA to be more effective if they anneal to the template DNA strand of transcribed genes and also increases the immunity mediated by crRNAs that anneal to the template strand of bacteriophage genomes through RNA-polymerase-mediated multi-turnover Cas9 nuclease activity. These data provide insights into the biology of the CRISPR system and provide a simple method of enhancing probability of successful genome editing by choosing sgRNAs that anneal to the template strand of DNA.

RESULTS

Active Transcription through Cas9 Target Sites Increases Genome Editing Frequencies

Several genomic factors that affect genome editing frequencies have been identified with previous studies, including nucleosome occupancy, DNase hypersensitive sites (DHSSs), and histone marks (H3K4me3) associated with active transcription (Chari et al., 2015; Horlbeck et al., 2016). To complement these findings using a distinct approach, we focused on being able to detect a large range of mutation frequencies as a way to identify genomic variables affecting Cas9-mediated mutagenesis. We examined a collection of 40 sgRNA, each targeting the coding sequence in a different gene (Table S1). Transient transfections were used to express Cas9 and an sgRNA in mouse embryonic stem cells (ESCs), genomic DNA was isolated 4 days after transfection, and indels were measured by targeted deep sequencing of each genomic target site. Analysis of these 40 sgRNA target sites revealed a wide range of indel frequencies (1.5% to 53.7%) (Figure 1A; Table S1). Most sgRNAs (33 of 40) displayed similar and high mutagenesis activity (>30% indel formation). Unexpectedly, the distribution of mutation frequencies was distinctly bimodal, with 7 of the 40 displaying substantially lower activity that separated them from the majority of sgRNAs (Figure 1A). Interestingly, six of the seven poorly performing sgRNAs annealed to the DNA strand that was not used by RNA polymerase II (Pol II) as the template for transcription (i.e., the non-template strand) (Figures 1B and 1C; Table S1). The seventh annealed to the template strand of a gene (*Actbl2*) that was not expressed in ESCs (Figures 1B and 1C; Table S1). For simplicity, sgRNAs that anneal to the non-template strand of a transcribed DNA will hereafter be referred to as non-template sgRNA, and those that anneal to the template strand of a transcribed DNA will be referred to as template sgRNA (Figure 1C).

To assess the correlation between transcription and indel mutagenesis with additional sgRNAs, the large dataset from Chari et al. was re-examined. The relationship between indel formation and template/non-template status of sgRNA was tested. Transcription through each targeted site was evaluated by RNA sequencing (RNA-seq) fragments per kilobase million (FPKM) levels from the same cell line (Figure S1A) (Chavez et al., 2015). Each target gene and its corresponding sgRNA were binned into quartiles based on FPKM values. High levels of gene transcription positively correlated with higher mutation frequency, with a significant (~2-fold) difference between quartiles 1 and 4 (Figure S1B, left). This effect from transcription appeared to be caused by increased efficiency from template sgRNA (Figure S1B, middle), because transcription levels did not generate statistically significant differences among the bins of non-template sgRNA (Figure S1B, right).

To directly test the effects of transcription through the Cas9 target site, we used a mouse ESC line harboring a doxycycline (dox)-inducible mCherry gene (Figure S1D). Twenty sgRNAs (12 template and 8 non-template) targeting the mCherry gene were first assessed for their ability to stimulate Cas9 digestion of DNA in *in vitro* reactions by generating each RNA individually then digesting an mCherry-containing plasmid (Figure S1C). All sgRNAs were able to stimulate DSB formation *in vitro*, although five (5, 11, 12, 14, and 16) required higher concentrations of Cas9 than the other 15 sgRNAs (Figure S1C). Mutagenesis frequencies mediated by the 20 sgRNAs *in vivo* were measured by T7 endonuclease 1 (T7E1) activities on PCR products generated from genomic DNA isolated 2 days after transfection (Figure S1E). Without dox-induced transcription of mCherry, the 20 sgRNAs displayed a range of indel formation (3%–21%), and the ranges of indel frequencies derived from template sgRNAs were not significantly different from those of non-template sgRNA (Figures 1D and S1E). Stimulating mCherry transcription with dox following transfection did not significantly affect mutagenesis mediated by any of the non-template sgRNAs (Figure 1D). By contrast, mutagenesis by 9 of 12 template-strand sgRNAs was significantly increased by transcription through the target site (Figure 1D). The stimulation of mutagenesis caused by transcriptional activity was substantial (2- to 3-fold) for those sgRNAs that were affected.

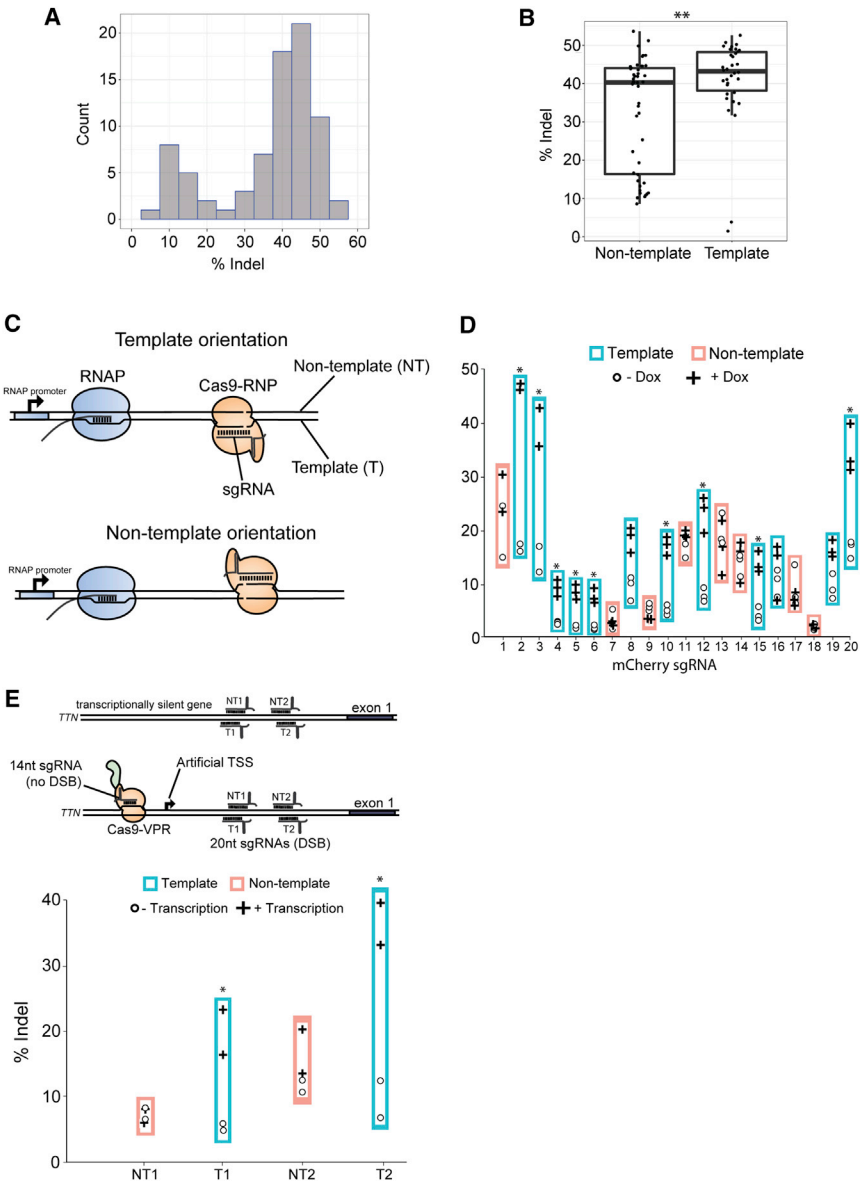

Figure 1. Transcription-Mediated Displacement of Cas9 from the DSB Increases Genome Editing Frequencies and Is Strand Dependent

(A) Bimodal distribution of indel frequencies of 40 distinct mouse genes 4 days after transient transfection of Cas9 and sgRNA expression plasmids. Individual observations from biological duplicates for each sgRNA were binned according to their mutation frequencies (% indel), and the number of sgRNAs that fell into each bin is displayed (count). See also Table S1.

(B) Indel frequencies associated with the 40 sgRNAs in (A) were separated by whether the sgRNA annealed to the DNA strand used as the template for transcription by RNA polymerase II (Pol II) or the non-template DNA strand. There are 17 template strand sgRNAs and 23 non-template sgRNAs. Each point represents a mutation frequency of independent transfections; n = 2 for each sgRNA. **$p < 0.01$.

(C) Schematic illustrating orientation of Cas9, target DNA, and an approaching RNAP for the two possible RNAP and Cas9 collision orientations (with a template sgRNA and a non-template sgRNA).

(D) Mutagenesis frequencies mediated by 20 different sgRNAs targeting a genomic mCherry measured by T7E1 assays (see also Figure S2E). mCherry transcription is controlled by doxycycline (dox) (see Figure S2D). Plus signs (+dox/mCherry expression) and circles (−dox / no mCherry expression) represent individual biological replicates testing the effect of transcription on mutagenesis levels mediated by each sgRNA. Genomic DNA was isolated 48 hr after transfection. *$p < 0.05$.

(E) The strand bias was tested at a silent endogenous gene through synthetically activating transcription of the human *TTN* gene using Cas9-VPR construct. Nuclease active Cas9-VPR was targeted to activate transcription, but not introduce DSBs, using a 14-nt sgRNA. Simultaneously, a 20-nt sgRNA targeted to either the template or non-template strand was provided to drive transcription mediated by 14nt-Cas9-VPR through Cas9 cleavage sites. Genomic DNA was harvest 48 hr after transfection, and mutation frequencies were analyzed via T7E1 assays. Each point represents a biological replicate.

The transcription-dependent template-strand effect on genome editing was tested on an endogenous gene in HEK293 cells by controlling the level of expression with a CRISPR-activation system. The system uses a truncated sgRNA using only 14 nt to target a nuclease active Cas9-VPR fusion protein to the *TTN* gene as previously described (Kiani et al., 2015). The truncated sgRNA is sufficient to stimulate transcription of *TTN* (Figure S1F), but it does not stimulate significant mutagenesis at that site (Kiani et al., 2015; Liao et al., 2017). The system enabled concomitant targeting of Cas9 nuclease by co-transfection with full-length sgRNAs, which were used to target sequences downstream of the transcriptional start site (Figure 1E). In the absence of the 14-nt sgRNA stimulating *TTN* transcription, the template and non-template sgRNAs displayed similar levels of indel mutagenesis (Figures 1E and S1G). Upon stimulation of *TTN* transcription with addition of the 14-nt sgRNA, indel frequency was stimulated by 2.5- to 4-fold for template sgRNAs, but not for non-template sgRNAs (Figures 1E and S1G).

Together, these results show that transcription through a Cas9 target site can stimulate mutagenesis in cells, provided the sgRNA anneals to the DNA strand that serves as the template for the RNA polymerase. We suggest that the transcription-mediated stimulation of mutagenesis prevents template sgRNAs from displaying weak indel mutagenesis activity. By contrast, non-template sgRNAs are more likely to provide weak activity, because they do not benefit from transcription through the target site. Mechanisms underlying this phenomenon are examined below.

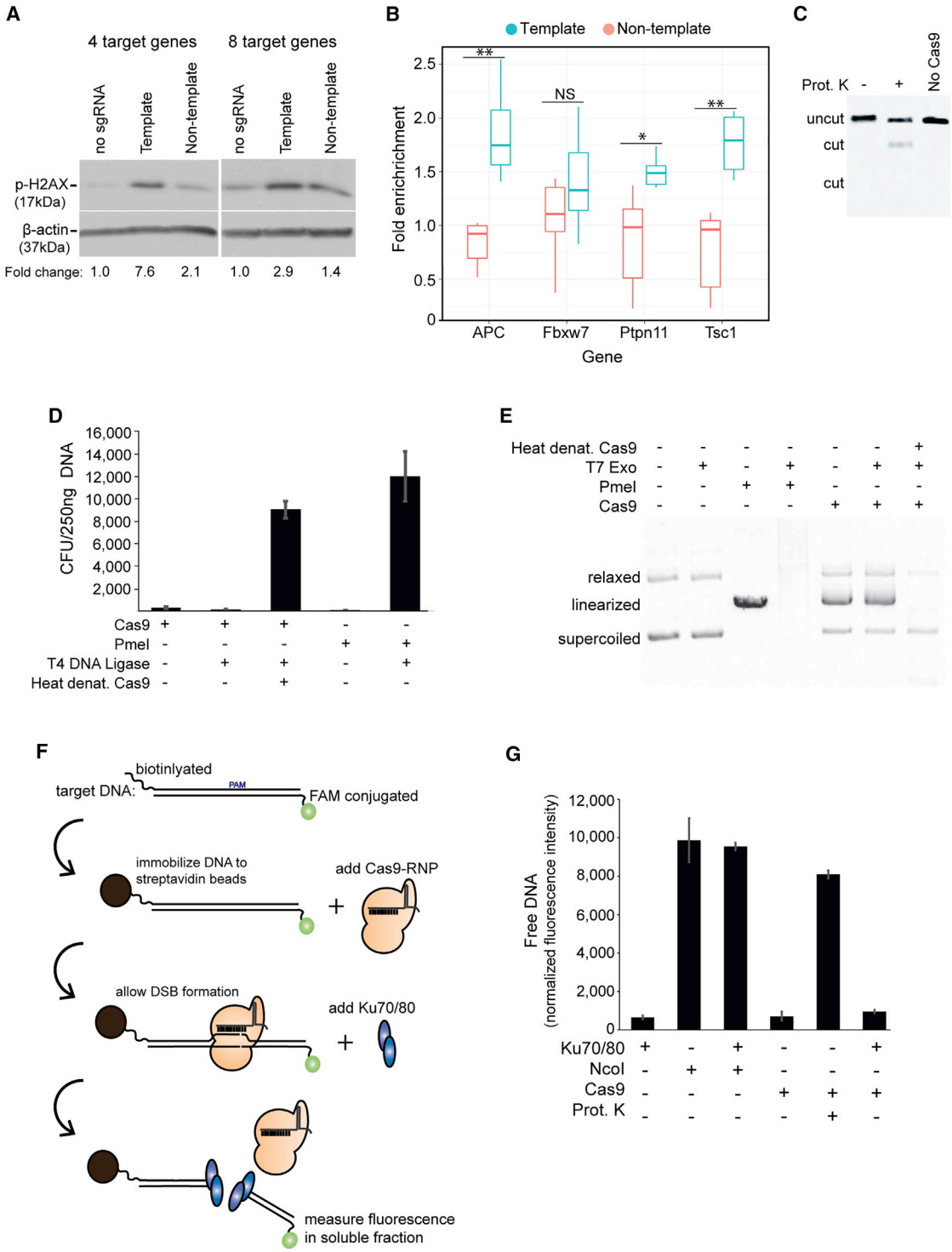

Figure 2. The Cas9-DSB Complex Precludes DNA Repair Activities

(A) Detection of phospo-H2AX levels 24 hr after transfecting mouse ESCs with pools of either template or non-template sgRNAs. sgRNAs that mediated >30% indel were selected (Figures 1A and 1B; Table S1). For each sgRNA, a new sgRNA annealing the opposite strand of the same gene was made. To compare strand among the same sets of genes, pools of 4 or 8 sgRNA consisted of the previously characterized and newly generated sgRNAs. Western blot analysis was used to determine fold change of phospo-H2AX signal with densitometric measurement of bands and normalization to the loading control (β-actin) and the no sgRNA control. Four target genes (*APC*, *FBXW7*, *PTPN11*, and *TSC1*) and eight target genes (*APC*, *FBXW7*, *PTPN11*, *TSC1*, *VPS16*, *VPS54*, *RAB7*, and *RANPBP3*) were used.

(legend continued on next page)

Cas9 Precludes DSB Repair Enzymes from Accessing DNA Ends

We tested the possibility that the different mutagenesis frequencies from non-template versus template sgRNA were caused by different levels of DNA repair. To determine if template sgRNAs elicited an elevated DNA repair response, multiple sgRNAs (either all template or all non-template) were transfected into cells with Cas9. We selected the sgRNA subsets (8 or 4 target genes) from the group of 40 (Table S1) where each of the sgRNAs generated >30% indel frequency after 5 days of expression (Figures 1A and 1B). Because each of these sgRNAs target a single gene and target one of the potential strands, we designed complementary sgRNAs that target the other strand for all genes in order to compare strand-biased effects on DNA repair activities generated by Cas9 at the same genes. 24 hr after transfection, protein lysates from cells were used for western blot analysis of phosphorylated histone 2AX, a marker for the cellular response to DNA damage and induction of DNA repair activity. Compared to the no-sgRNA control, the non-template sgRNA pools generated a relatively modest (1.4- to 2.1-fold for 8 and 4 genes, respectively) stimulation of H2AX phosphorylation (Figure 2A). The template sgRNAs were significantly more effective at stimulating H2AX phosphorylation (2.9- to 7.6-fold for 8 and 4 genes, respectively) in cells, suggesting a higher frequency of DNA repair occurring in cells with template sgRNA.

The onset of DNA repair at the Cas9 target site was examined with chromatin immunoprecipitation (ChIP) assays using antibodies specific for Ku70/80 DNA end-binding proteins. As an early step in non-homologous end joining (NHEJ) repair of DSBs, binding of Ku70/80 at Cas9 target sites was used to assess whether template sgRNAs were more effective at stimulating repair than non-template sgRNAs. The set of four template or non-template sgRNAs was co-transfected with Cas9 in mouse ESCs, proteins were crosslinked to DNA after 24 hr, and chromatin was subjected to Ku70/80 ChIP assays. Three (APC, Ptpn11, and Tsc1) of the four template sgRNAs significantly increased Ku70/80 binding compared to control genomic sites (Figure 2B). By contrast, none of the non-template sgRNAs significantly increased Ku70/80 binding in transfected cells (such that it was detectable with this ChIP assay). The results of this assay are consistent with increased frequency of DNA repair occurring at template sgRNAs compared to non-template sgRNAs.

Previous biochemical experiments demonstrated that Cas9 remains tightly associated with DNA after generating a DSB (Jinek et al., 2014; Nishimasu et al., 2014; Richardson et al., 2016). Consistent with this property, *in vitro* Cas9 nuclease reactions (as in Figure 1D) required removal of Cas9 with proteinase K in order visualize the migration of DNA products into an agarose gel by electrophoresis (Figure 2C). *A priori*, it is not known if any endogenous activity indeed displaces Cas9 from genomic DSBs, but Richardson and colleagues showed that challenging the enzyme-product complex with ssDNA displaced Cas9 from the DSB *in vitro* and also simulated mutagenesis in cells, but only when the ssDNA was complementary to the non-target, PAM-distal strand (Richardson et al., 2016). Although a variety of DNA metabolic activities, including nucleosome remodeling and DNA replication, may be capable of displacing Cas9 from DSBs, those activities are difficult to predict or control in a genomic-site-specific manner. By contrast, the direction of RNA polymerase through a gene is well annotated throughout the genome and can be experimentally controlled. Interestingly, the asymmetry in the ability of ssDNA to displace Cas9 from the DSB is consistent with Cas9 being more sensitive to collisions in the template strand orientation compared to the non-template strand orientation (described more extensively below) (Richardson et al., 2016). Therefore, we posited that the strand bias has differing effects on persistent binding of Cas9 to the DSB, leading to the difference in observed phospho-H2AX signals (Figure 2A) and Ku70/80 binding (Figure 2B). Furthermore, we hypothesized that the Cas9-DSB complex directly prevents DNA repair activities, thus making removal of Cas9 an important step for efficient genome editing.

To begin to test this hypothesis, we determined if persistence of Cas9 binding to DNA prevents DNA end-binding proteins from accessing the Cas9-generated DSB *in vitro*. We tested whether T4 DNA ligase could evict Cas9 from the DSB by first forming Cas9-DSB complexes on a circular plasmid DNA and then

(B) Differences in Ku70/80 binding at template or non-template Cas9-generated DSBs was measured by ChIP of Ku70/80-bound DNA followed by qPCR. ChIP DNA was isolated 24 hr after transfection of DNA to express the pool of four sgRNAs from (A). DNA precipitated by Ku70/80 antibodies at each target site was measured through qPCR amplifying a sequence adjacent to each Cas9 cleavage site. For each transfected cell population, two biological replicates were harvested, and each was split into three technical replicates prior to immunoprecipitation. Data are expressed as enrichment of the target site compared to the negative control site (*Gapdh*). $^{**}p < 0.01$, $^{*}p < 0.05$.

(C) Agarose gel electrophoresis of an *in vitro* reaction where linear dsDNA was digested by Cas9 for 30 min and then treated with Proteinase K to release the cleaved DNA products.

(D) The ability of T4 DNA ligase to repair a Cas9-generated DSB in a circular plasmid DNA was measured through *E. coli* colony formation on ampicillin-containing plates (CFU) after transformation. Cas9 or restriction endonuclease (PmeI) digestion of plasmid DNA prevented CFU following transformation. T4 DNA ligase activity repaired the DSB and stimulated CFU if plasmid was cut with PmeI or if Cas9 was denatured at 75°C for 10 min before addition of ligase. T4 DNA ligase did not stimulate CFU if Cas9 was not denatured. Values represent mean ± SD; n = 3.

(E) Agarose gel analysis of a circular plasmid DNA incubated with T7 exonuclease and the conditions indicated above each lane. PmeI and heat denaturation of Cas9 were as described in (D). Cas9 prevented DNA ends from serving as a substrate for T7 exonuclease unless reactions were heat denatured prior to exonuclease addition. All reactions were treated with Proteinase K before gel loading.

(F) Schematic depicting the experiment in (G) to test if Ku70/80 can displace Cas9 from its DSB. The Cas9-DSB complex is formed on target DNA that is biotinylated on one end and fluorescein (FAM) conjugated on the other. If purified human Ku70/80 displaces Cas9 from the DSB, release of the fluorescent DNA end is measured as soluble fluorescence.

(G) Liberation of fluorescent DNA ends into the soluble fraction after challenging the target DNA with indicated conditions. NcoI is a restriction endonuclease that cuts the DNA substrate and functions as the control for maximum fluorescence, and maximum fluorescence of Cas9-digested DNA was assessed through Proteinase K treatment after Cas9-DSB formation. See also Figure S2D. Values represent mean ± SD; n = 3.

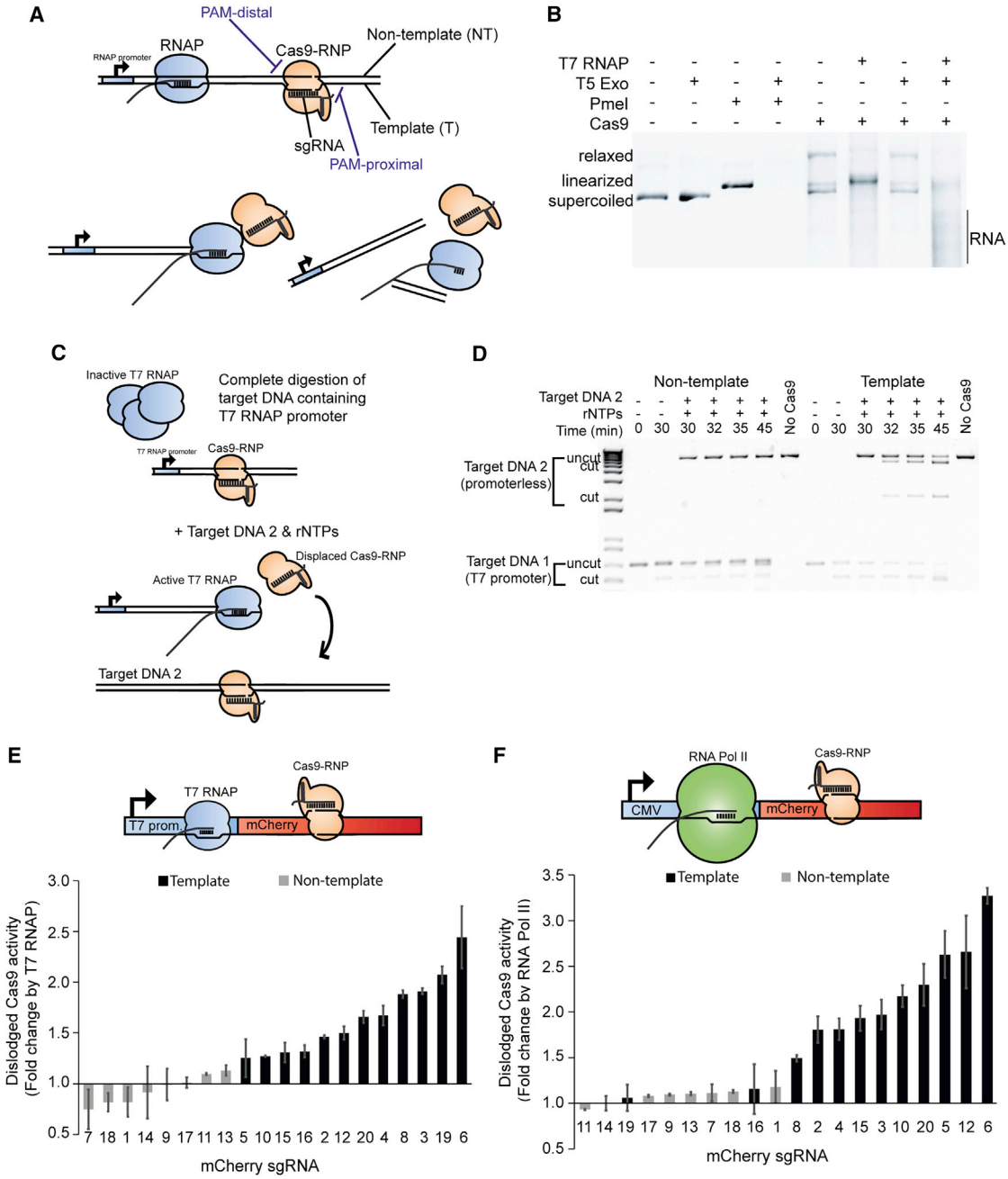

Figure 3. The Cas9-DSB Complex Is Disrupted by Translocating RNAPs if the sgRNA Anneals to the Template Strand

(A) Schematic illustrating orientation of Cas9 RNP, target DNA, and T7 RNAP translocation colliding with the PAM-distal surface of Cas9 for a template sgRNA and disruption of the enzyme-product complex.

(B) DNA degradation by T5 exonuclease ability to access Cas9-generated DSB ends in the presence or absence of T7 RNAP transcription was visualized by agarose gel electrophoresis. Plasmid DNA harboring a T7 promoter was digested with Cas9 or PmeI restriction endonuclease for 30 min prior to incubation with T5 exonuclease and/or T7 RNAP. All reactions were treated with Proteinase K before gel loading.

(C) Schematic illustrating experiment in (D) to test whether T7 RNAP can evict Cas9 from the DSB and whether T7 RNAP-displaced Cas9 molecules retain activity. In the presence of inactive T7 RNAP, the Cas9-DSB complex was formed on a target DNA 1, which contains a T7 RNAP promoter on either end of the DNA for either collision orientation. After 30-min incubation, rNTPs and a second substrate (target DNA 2) are simultaneously added. Target DNA 2 lacks a T7 promoter. Target DNA 1 and target DNA 2 each have the same DNA sequence targeted by Cas9. The addition of rNTPs and target DNA 2 stimulates T7 RNAP transcription and provides a sensor of displaced Cas9 molecules.

(D) Agarose gel for the experiment described in (C). Template and non-template refer to the location of the T7 promoter on target DNA 1. Cleavage of target DNA 2 indicates displacement of active Cas9 from target DNA 1 over time.

(legend continued on next page)

adding T4 DNA ligase and incubating at 16°C before using the reactions for bacterial transformation into *E. coli*. A lack of antibiotic-resistant colonies indicated that the ligase was unable to access and repair the Cas9-bound plasmid that encoded ampicillin resistance (Figure 2D). Removing Cas9 by a brief heat denaturation before the ligase reaction restored colony formation, demonstrating that the Cas9-generated DSB was a competent substrate for T4 DNA ligase if Cas9 was removed from the DNA (Figure 2D). DNA exonuclease activity was examined by comparing degradation of a circular DNA linearized by either a restriction endonuclease or by Cas9 (Figure 2E). Exonuclease activity was prevented at the Cas9-generated DNA ends, unless Cas9 protein was removed by heat denaturation (Figure 2E). These indicate that the persistence of the Cas9-DSB complex prevents the DNA ends from being used as substrates for DNA repair enzymes.

To test whether mammalian DSB end-binding proteins could evict Cas9 from its DSB, Cas9 was targeted to a DNA that was immobilized on a bead at one end and fluorescently tagged at the other end. Disruption of the Cas9-DSB complex was detected by measuring soluble fluorescence (Figure 2F). As a positive control, Cas9-digested DNA was treated with proteinase K to release the fluorescent tag from the bead. When challenging the Cas9-DSB with purified human Ku 70/80, a 100× molar excess of the Ku70/80 complex was incapable of displacing Cas9 from the DSB (Figure 2G), despite Ku70/80 binding to the other DNA ends present in the reaction (Figure S2C). Although these *in vitro* observations use a DNA substrate that is not subjected to events occurring on genomic DNA in cells, they demonstrate that the persistent Cas9 binding to DNA can cause the DSB to be inaccessible to DNA end-binding proteins. This property is consistent with the possibility that perdurance of Cas9-DSB complex constitutes a rate-limiting step during genome editing *in vivo*.

The Cas9-DSB Complex Is Disrupted by Translocating RNA Polymerases

We hypothesized that transcription through a Cas9 site increases indel formation, because a translocating RNA polymerase dislodges Cas9 from its DSB (diagramed in Figure 3A). Removing Cas9 from the DSB could stimulate mutagenesis by decreasing the time it takes for the DNA ends to become accessible to cellular repair machinery. To determine if RNA polymerase (RNAP) translocation through the Cas9 site was sufficient to make the DSB accessible to other proteins, we utilized a dsDNA Cas9 substrate harboring the T7 promoter upstream of the cleavage site. The promoter and Cas9 site were orientated so that the sgRNA annealed to the DNA strand that was used as the template by T7 RNAP for transcription. A combined reaction was performed wherein Cas9 digestion of the DNA occurred at the same time as T7 RNAP transcription of the same DNA (Figure 3B). T7 RNAP transcription through the Cas9 site allowed the DSB to be effective substrates for T5 exonuclease activity to degrade the DNA (Figure 3B). This result indicated that translocation of a T7 RNAP through the Cas9-DSB complex made the DNA ends accessible.

The DNA strands emanating from one side of the Cas9-DSB complex display more freedom than DNA from the opposite side. As mentioned above, DNA at the PAM-distal surface of Cas9 (Figure 3A) is vulnerable to dissociation when challenged, whereas DNA at the PAM-proximal surface of Cas9 is not (Richardson et al., 2016). The 5′ to 3′ direction of RNA polymerization causes a translocating RNAP to collide with PAM-distal surface of the Cas9-DSB when the sgRNA anneals to the DNA strand used as a template by RNAP (as displayed in Figure 3A). Conversely, when the sgRNA anneals to the non-template strand, translocation of the RNAP will result in a collision with the PAM-proximal surface of the Cas9-DSB complex. We hypothesized that these differences could affect genome editing *in vivo* if the orientation of the collision affected the ability of RNAP to disrupt the Cas9-DSB complex.

To test a strand bias in the ability of RNAP to dislodge Cas9, we developed an assay that took advantage of the dislodged Cas9-RNP possibly being able to bind to another DNA molecule and generate a DSB in that DNA as long as it contained the sgRNA target sequence. First, Cas9 and a T7-promoter-containing target DNA (target DNA 1) were incubated (30 min) to allow DNA cleavage and formation of the Cas9-DSB complex. Next, a promoterless target DNA (target DNA 2) containing an identical Cas9 target site was added (Figure 3C). Note that a 10-fold molar excess of target DNA 1 relative to Cas9 and stability of the Cas9-DSB complex combined to prevent detectable cleavage of target DNA 2 in the absence of transcription (Figure 3D). Transcription through the Cas9-DSB complex in target DNA 1 was activated by adding ribonucleoside triphosphates (rNTPs), and we began measuring cleavage of target DNA 2 after 2 min of transcription. Target DNA 2 was cut rapidly after initiating transcription, but only if the sgRNA bound to target DNA 1 was annealed to the template strand (Figure 3D, right side). Collision with Cas9-DSB in the non-template orientation did not generate nuclease activity on target DNA 2 (Figure 3D, left side). Since target DNA 2 was not transcribed in this assay, the stimulation of its digestion by T7 RNAP could not be caused by a differential activity of Cas9 on actively transcribed DNA per se. The rapid digestion of target DNA 2 after RNAP activation is most consistent with RNAP activity on target DNA 1 removing Cas9 from its DSB, and allowing it to digest another DNA molecule. Finally, the inability of T7 RNAP to stimulate target DNA 2 digestion in the non-template sgRNA orientation is consistent with Cas9-DSB complexes being resistant to dissolution by RNAP colliding

(E) The ability of T7 RNAP to displace Cas9 with various sgRNAs was measured similar to (C), except target DNA 2 was biotinylated on one end and FAM conjugated on the other end, as illustrated in Figure S2D. The 20 mCherry sgRNAs (from Figures 1D and S1C) were subjected to the assay in the presence or absence of rNTPs. The fold change in fluorescence levels as a result of T7-RNAP-mediated displacement was measured through fluorescence in the soluble fraction. Values are mean ± SD; n = 3 for each sgRNA.

(F) Fold-change Cas9 activity dislodged from mCherry DNA by mammalian Pol II activity from nuclear extracts. Activity was measured by the soluble fraction fluorescent levels for a fluorescent as above. Pol II activity was controlled by addition of α-amanitin. See also Figure S2D. Values are mean ± SD; n = 2 for each sgRNA.

with the PAM-proximal surface of Cas9. Together, these data indicate that the Cas9-DSB complex can be disrupted by RNAP if the sgRNA anneals to the template strand.

We examined whether the strand-biased ability to displace Cas9 *in vitro* was a general phenomenon by measuring displacement levels for the 20 sgRNAs targeted across a linear mCherry substrate. Reactions were performed in the presence or absence of rNTPs to compare transcription mediated displacement levels for each sgRNA. Displacement of Cas9 activity from a T7-containing mCherry DNA was measured using an immobilized, fluorescently tagged target DNA 2. After completion of the combined digestion and transcription reaction, displacement was assessed by fold change in soluble fluorescence stimulated by RNAP (Figures 3E and S2D). These reactions showed that all template-annealed sgRNAs were compatible with displacement by T7 RNAP (Figure 3E). In contrast, all of the non-template sgRNAs were recalcitrant to displacement (Figure 3E).

T7 RNAP and mammalian Pol II can be considered very different from each other in terms of their biophysical and biochemical properties. Since the *in vitro* results elucidated above used T7 RNAP, but we propose that the *in vivo* genome editing effects of transcription are cause by Pol II, the ability of Pol II to displace Cas9 from its DSB was determined. A fluorescent displacement assay was performed essentially as described above for the T7 RNAP experiment (Figures 3E and S2D); however, target DNA 2 was used to detect Cas9 dislodged off of a CMV-mCherry template by Pol II activity from mouse ESC nuclear extracts (Figures 3F and S2E). To determine dependence of transcription for Cas9 displacement, reactions were performed in the presence or absence of the Pol II/III inhibitor α-amanatin (Figure S2E). Fold changes in fluorescence levels revealed that none of the eight non-template sgRNAs were significantly displaced (Figure 3F). Thus, the non-template sgRNA prevented displacement of Cas9 from DSBs for either RNAP tested. By contrast, 10 out of 12 template sgRNAs were substantially displaced by Pol II activity (Figure 3F). Interestingly, template sgRNAs displayed varying levels of displacement in both transcription scenarios, suggesting sgRNA-determined variability in disruption of the Cas9-DSB complex. Notably, two template sgRNAs (16 and 19) were not displaced by Pol II activity, and a third (8) displayed a low level of displacement relative to other template sgRNA. Levels of indel mutagenesis with these three template sgRNAs did not significantly increase after transcriptional activation of mCherry *in vivo* (Figure 2E). Together, these data indicate that a strand-biased Pol II displacement of Cas9 from its DSB stimulates indel mutagenesis in cells.

RNAP Can Convert Cas9 into a Multi-turnover Nuclease

When using Cas9 for genome editing in cells or organisms, the nuclease is typically expressed or delivered at a high molar ratio relative to its DNA substrates, which are often only 2–4 copies per cell. As such, efficiency of genome editing is likely less dependent on the capabilities of one Cas9 nuclease to processively digest many DNA substrates than it is on a rapid detection of the DSB by the cell's repair machinery. However, when RNAP collides with the Cas9-DSB complex, the displaced Cas9 molecule retained its nuclease activity (Figures 3B and 3D), suggesting that Cas9 could be converted from a single-turnover nuclease to a multi-turnover nuclease. An ability of a single Cas9 molecule to digest many DNA substrates could be important when saturating levels of DNA targets need to be digested, such as when high multiplicities of infection occur during bacteriophage infection.

To determine the multi-turnover capabilities of Cas9, a 2-fold excess of a single, T7-promoter-containing target DNA was used as a substrate for *in vitro* Cas9 digestion reactions. To test template and non-template orientations using the same sgRNA, the promoter was placed on either end of the target DNA. After an initial 30-min digestion of half of the DNA, addition of rNTPs was used to initiate T7 RNAP activity, and RNAP-stimulated cleavage of DNA was measured for up to 30 min (Figure 4A). Placing the T7 promoter so that the sgRNA annealed to the template strand stimulated Cas9 cleavage activity with rapid kinetics similar to those observed at the start of a reaction (Figures 4A and S3A). No stimulation was observed with the non-template strand orientation (Figure 4A). Continual displacement of Cas9 by T7 RNAP did not appear to disrupt the Cas9-sgRNA interaction, because Cas9 did not exchange sgRNA molecules after being displaced (Figure S3B).

Altering the amount of Cas9 (Figure 4B) or the amount of T7-promoter-containing DNA substrate (Figure 4C) in a reaction revealed substantial capabilities of Cas9 to function as a multi-turnover nuclease *in vitro*. Diluting Cas9 showed that T7 RNAP increased the capacity for template sgRNA orientation by 10-fold compared to reactions without T7 RNAP translocation through Cas9, which functioned as a single-turnover nuclease (Figures 4B and S3C). The improved capacity increased kinetics of Cas9 activity at saturating substrate concentrations (Figure 4C). T7 RNAP converted Cas9 to a multi-turnover nuclease for a variety of sgRNAs and target DNAs tested, but only when the sgRNA annealed to the template DNA strand (Figures 4D, S4A–S4C, and S6). The magnitude of stimulation by T7 RNAP varied among template sgRNAs, but it did not appear to correlate with GC content of the target site (Figure S4D) or the GC content in the sequence next to the PAM (Figure S4E). In summary, when combined with T7 RNAP and sgRNA in the template strand orientation, Cas9 was effectively transformed from a single-turnover enzyme into a multi-turnover enzyme.

PAM Sequences and Protospacer Targets Are More Frequently Located on Template Strand of *Streptococci* Phages

We wondered whether the strand bias in Cas9's potential to act as a multi-turnover nuclease contributed to bacterial immunity. Given a stoichiometry of multiple bacteriophage particles infecting individual bacterial cells, we reasoned that Cas9 functioning as a multi-turnover nuclease could have substantial benefits over a single-turnover nuclease. A multi-turnover nuclease could significantly enhance bacteriophage immunity by allowing a single Cas9 molecule to destroy more than one bacteriophage genome. Therefore, we examined whether there were differences in the frequencies of Cas9 predicted to act as a single-turnover versus multi-turnover nuclease on bacteriophage genomes.

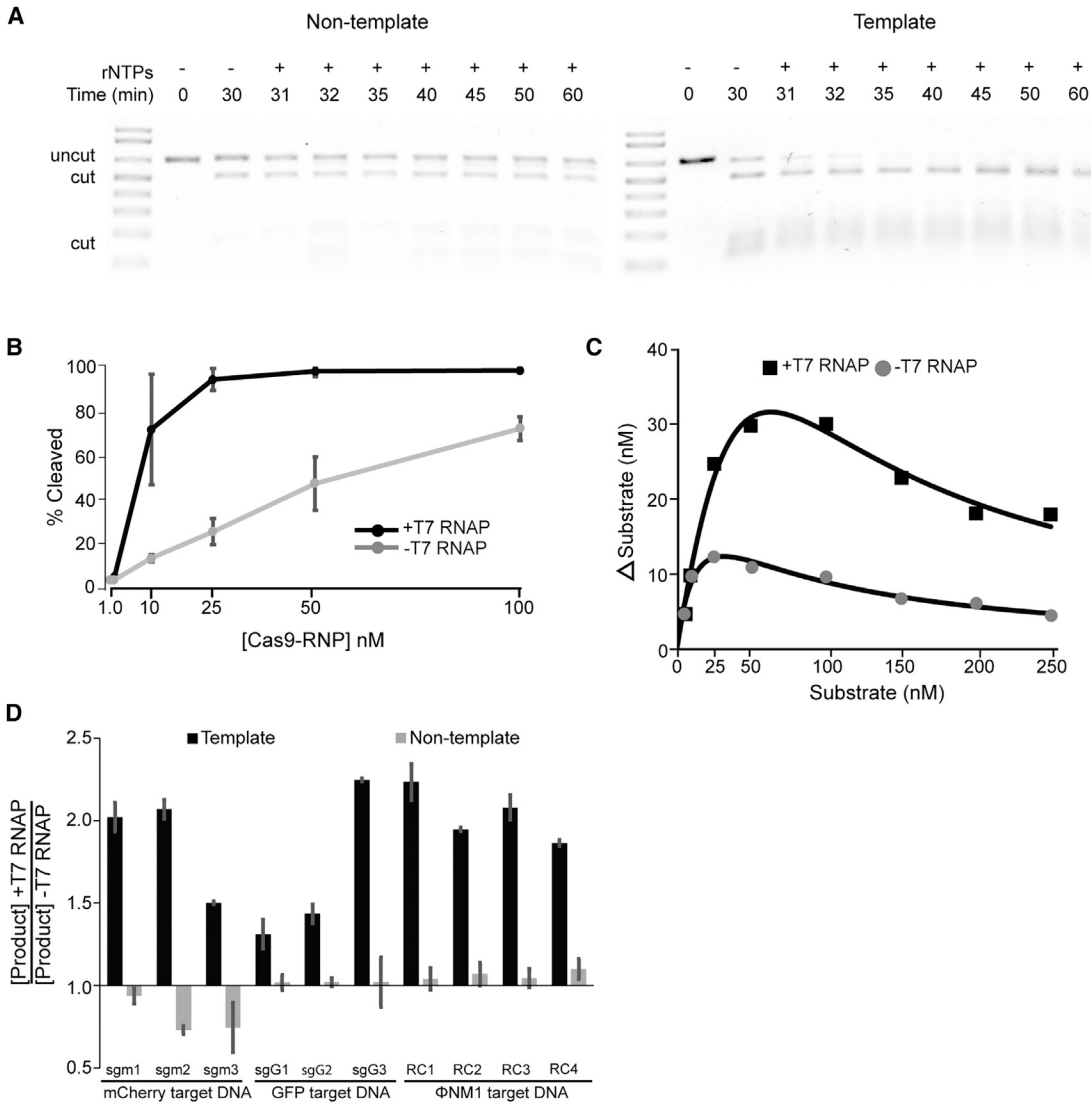

Figure 4. Strand-Dependent Ability of Translocating T7 RNAP to Stimulate *In Vitro* Multi-turnover Nuclease Activity by Cas9

(A) Multi-turnover nuclease capability of Cas9 was visualized by agarose gel analysis of hybrid reactions combining Cas9 nuclease and T7 RNAP transcription reactions. A T7 promoter was placed on either end of the target DNA to achieve template or non-template orientation. Cas9 was incubated with DNA for 30 min as shown before initiating T7 RNAP with addition of rNTPs.

(B) The multi-turnover capacity of template strand Cas9 was measured through titration of in the presence or absence of T7 RNAP. Target DNA was held constant at 150 nM. Values represent mean ± SD; n = 3. See also Figure S3C.

(C) Titration of substrate in the presence or absence of T7 RNAP. Cas9 was held constant at 12.5 nM. Values represent mean ± SD; n = 2. See also Figure S3D.

(D) Multi-turnover Cas9 activity on various sgRNAs was examined through hybrid digestion and transcription reactions of target DNAs harboring T7 RNAP promoters in the template or non-template strand orientation. See also Figure S4A for schematics and Figures S4B, S4C, and S6 for representative gels. Values represent mean ± SD of fold changes in cleavage by indicated sgRNAs in the presence or absence of T7 RNAP; n = 3.

Interestingly, the nucleotide composition of bacteriophage genomes differs in the DNA strand replicated by leading-strand versus lagging-strand DNA synthesis (Jin et al., 2014; Kwan et al., 2005; Lobry, 1996; Uchiyama et al., 2008). This phenomenon has been named GC skew, and underlying causes for it remain uncertain. For Streptococcus phages that infect *S. pyogenes* and *S. thermophilus*, the GC skew is reflected in the nucleotide composition of the plus strand (34% adenine/27% threonine and 22% guanine/17% cytosine). The structure of these bacteriophage genomes places the transcription of genes in predominantly one direction; thus, template strands have a different nucleotide composition than non-template strands. Consequently, the potential PAM sites for spCas9 (NGG) and *S. thermophilus* Cas9 (stCas9; NNAGAAW) are not strand neutral. Instead, they preferentially target the template strand at about a 2:1 ratio for spCas9 and 3:1 ratio for stCas9 (Figures 5A, 5B, and S5A). Mapping crRNA identified from bacteriophage-insensitive mutant strains to bacteriophage

A

	PAM	# Template	# Non-Template	% Template
phage 2972: 34704bp	NNAGAAW	179	52	77.5%
	NGG	1450	777	65.1%
phage 128: 34593bp	NNAGAAW	108	45	70.6%
	NGG	1381	833	62.4%
phage 73: 36377bp	NNAGAAW	183	63	74.4%
	NGG	1467	793	64.9%
phage 53: 34239bp	NNAGAAW	166	69	70.6%
	NGG	1381	807	63.1%
phage 858: 35543bp	NNAGAAW	169	64	72.5%
	NGG	1476	758	66.1%
phage 5093: 37184bp	NNAGAAW	219	96	69.5%
	NGG	1329	714	65.1%
phage 7029: 35466bp	NNAGAAW	176	93	65.4%
	NGG	1371	794	63.3%
prophage 20167: 48800bp	NNAGAAW	302	117	72.1%
	NGG	1999	1115	64.2%
phage Sfi11: 39807bp	NNAGAAW	209	84	71.3%
	NGG	1544	802	65.8%
phage Sfi19: 37307bp	NNAGAAW	190	95	66.7%
	NGG	1516	822	64.8%
phage Sfi21: 40793bp	NNAGAAW	222	108	67.3%
	NGG	1520	896	62.9%
prophage TP-778L: 41757bp	NNAGAAW	200	81	71.2%
	NGG	1600	920	63.5%
prophage TP-J134: 45606bp	NNAGAAW	226	91	71.3%
	NGG	1711	967	63.9%
phage NM4: 40365bp	NNAGAAW	286	80	78.1%
	NGG	1406	624	69.3%
phage NM1: 43219bp	NNAGAAW	303	105	74.3%
	NGG	1387	688	66.8%
phage A25: 33900bp	NNAGAAW	173	52	76.9%
	NGG	1472	779	70.9%
phage T12: 37976bp	NNAGAAW	164	67	72.9%
	NGG	1431	798	63.6%

B

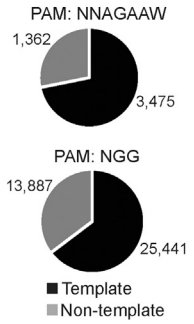

Figure 5. PAM Sequences across *Streptococci* Phage Are More Frequently Oriented on the Template Strand

(A) Of the 16 surveyed *Streptococcus* phages, all harbor the majority of the PAM sequences on the DNA strand corresponding to the transcription template strand. NNAGGAW, *S. thermophilus* PAM; NGG, *S. pyogenes* PAM.

(B) Distribution of all PAM sequences among genomes analyzed in (A).

genomes showed that the actual frequency of crRNAs annealing to the template strand are more abundant than those annealing to the non-template strand (Figure S5B; Table S3) (Achigar et al., 2017; Levin et al., 2013). Thus, the combination of the GC-skew, bacteriophage genome structure, and the PAM sequence results in CRISPR targeting Cas9 to bacteriophage more frequently in a multi-turnover orientation. Rational engineering of Cas9 proteins showed that mutagenesis can relatively simply change the PAM sequence that Cas9 recognizes (Kleinstiver et al., 2016), indicating that the nuclease has potential to be preferentially targeted to either or neither strand in bacteriophage genomes. Based on the above correlations, we hypothesized that targeting Cas9 to anneal to the bacteriophage template strand provides a selective advantage by allowing Cas9 to function as a multi-turnover nuclease during active transcription through target sites.

Template-Targeted Protospacers Enhance Bacterial Adaptive Immunity

To directly test a strand bias effect on bacterial immunity, we used two virulent versions of the ΦNM1 phage. One contains a mutation that inactivates the promoter required for transcription of the lysogeny cassette (ΦNM1γ6) (Goldberg et al., 2014). The other expresses the lysogeny cassette, but it harbors an inactivating deletion within the cI repressor gene (ΦNM1h1) (Figure 6A). Therefore, neither phage can establish lysogeny, but they differ in the transcription of the lysogeny cassette.

To test the effect of transcription through a Cas9 target site, we generated different bacterial strains harboring spacers annealing to either template or non-template strand sequences within the repressor gene found in both ΦNM1γ6 and ΦNM1h1 (Figure 6A). Each strain was infected with each phage, and their survival was determined by measuring optical density 600 (OD_{600}) over time (Figure 6B). The interference efficiency of each spacer against the two phages was interpreted from plate-reader growth curves of infected bacterial cultures. The two spacers targeting the non-template strand (RC2 and RC4) showed similar interference against either phage regardless of whether transcription was active (ΦNM1h1) or inactive (ΦNM1γ6). On the contrary, spacers targeting the template strand (RC1 or RC3) were notably more effective at providing immunity against the actively transcribed target (ΦNM1h1) than the inactive target (ΦNM1γ6). The same four target sites within ΦNM1 were tested for the ability of T7 RNAP translocation to turn Cas9 into a multi-turnover nuclease *in vitro* (Figure S6), demonstrating the template strand bias effect on the phage genome. These results show that active transcription across Cas9 targets improves CRISPR immunity by converting Cas9 into a multi-turnover enzyme, but the effect appears to be restricted to Cas9 annealed to the template strand.

DISCUSSION

The consequences of the persistent Cas9-DSB state were elucidated by identifying conditions that dissociate Cas9 from its DNA products. The stable enzyme-product complex precludes DNA repair activities, but it can be disrupted by translocating RNAPs in a strand-biased manner, conditionally converting Cas9 into a multi-turnover nuclease. This dislodging from the DSB had significant effects on genome editing and bacterial immunity by increasing mutation frequencies in mammalian cells and mediating enhanced phage interference through multi-turnover nuclease activity.

Although this study focuses on the effects of RNAPs on the Cas9-DSB complex, other activities involving DNA translocating proteins or DNA metabolism are also likely to effect removal of Cas9 and mutagenesis at the DSB. The ability of non-template sgRNAs to direct even low levels of mutagenesis ostensibly demonstrates that Cas9 in this orientation gets displaced from its DSB. The process of DNA synthesis is certainly sufficient to generate force needed to dislodge Cas9 from a DSB, and

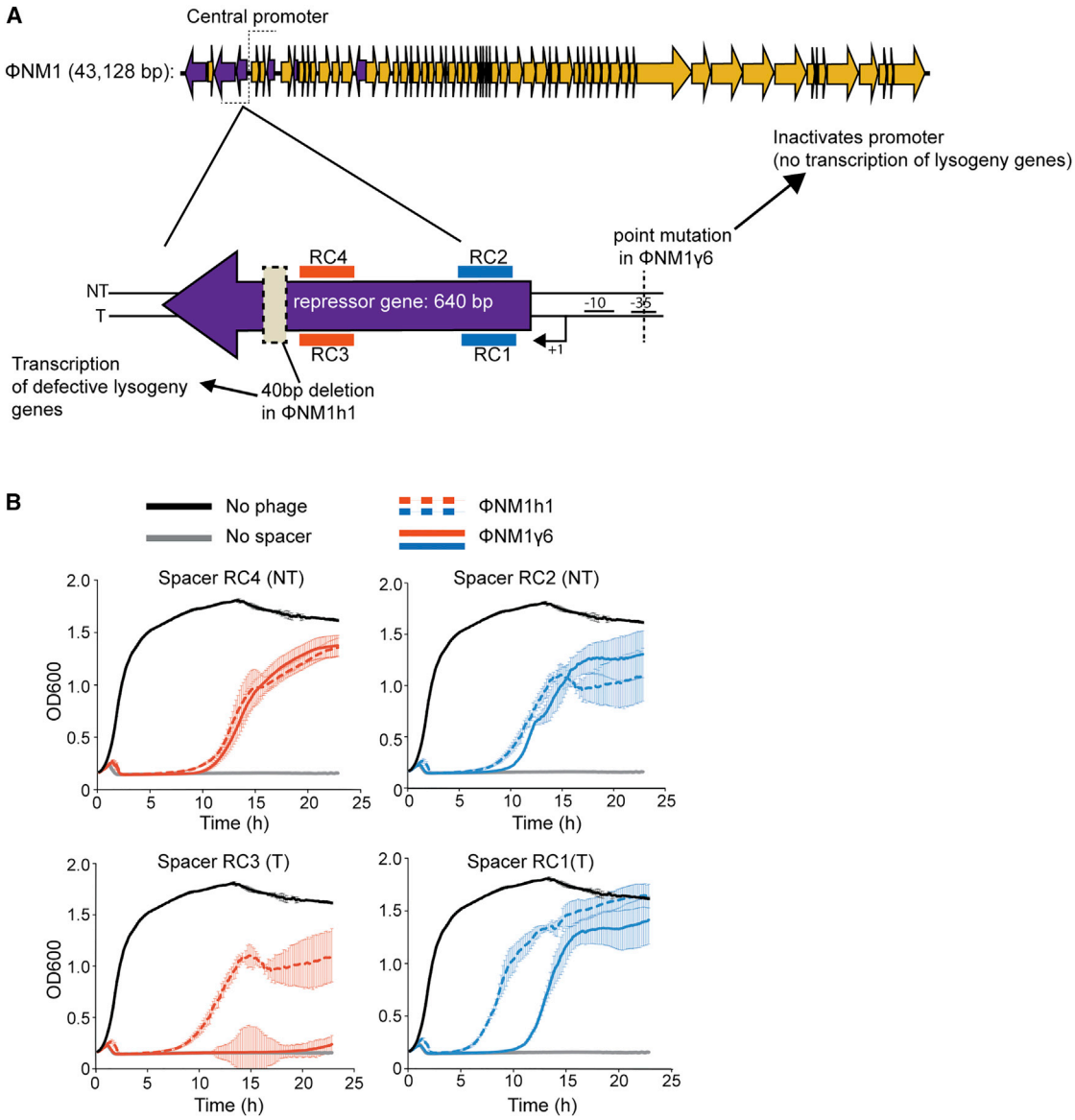

Figure 6. Template Strand-Targeted Protospacers Enhance Phage Interference

(A) General organization of the phage ΦNM1 genome and targeting strategy of the lysogenic repressor gene in the ΦNM1h1 and ΦNM1γ6 mutant phages. The ΦNM1h1 mutant has defective lysogeny genes that transcriptionally active, while the ΦNM1γ6 mutant has transcriptionally silent lysogeny genes. 2 pairs of protospacers were designed to target the mutant phages so that each pair consists of crRNA annealing to either the template or non-template strand with PAM sites within 25 bp of each other. *S. aureus* strains harboring *S. pyogenes* Cas9 and each of these spacers (RC1–4) were generated respectively for the experiment. (B) Growth curves of *S. aureus* strains harboring spacers RC1–4 after infection with ΦNM1h1 or ΦNM1γ6. T, template strand orientation; NT, non-template strand orientation.

individual DNA helicases may also be capable of removing Cas9. In contrast to these other DNA metabolic activities, translocation of RNAP is well annotated across mammalian genomes. In addition, the frequency of interactions is significantly different; multiple RNAP molecules translocate a site in a highly expressed gene, which encounters DNA replication machinery only once per cell division. We suggest the frequency is important, because blunt-ended Cas9 DSBs are frequently repaired in an error-free manner; therefore, iterative break-repair cycles are required for high mutation rates in Cas9-treated cells. In practice, low mutation rates can be overcome by continuous Cas9 activity over long time periods; however, doing so will increase the probability of off-target mutations and should be avoided.

This new understanding of the interaction between Cas9 and RNAPs can be directly applied to CRISPR-Cas9-based genome editing procedures. Our sample of 20 sgRNA to the same gene demonstrates that all these sgRNAs are competent

to mediate Cas9 digestion of substrates *in vitro*, yet they displayed substantial variability for indel frequency *in vivo*. Genomic factors, such as nucleosome occupancy, have previously been shown to affect indel frequency (Horlbeck et al., 2016); however, they are unlikely to affect variability here, because all sgRNA targeted a single locus, which should not vary in any of the previously identified factors. Instead, a large degree of variability among sgRNAs was clearly attributable to the direction of Pol II translocation through the Cas9 target site. Although the 2- to 3-fold increased mutagenesis should be considered substantial, more benefit to genome editing will likely be gained by reducing the probability of using a so-called dud sgRNA by avoiding non-template sgRNAs. Subsequent research resulting in the modification of Cas9 or discovery of small molecules that destabilize the Cas9-DSB complex could stimulate CRISPR-Cas9-based mutagenesis, especially at non-transcribed sites and in cells with low DNA metabolic activity. In the absence of such advances, our findings provide a simple and straight-forward path for increasing efficiency of Cas9-mediated mutagenesis, which is to preferentially use only sgRNAs that anneal to the template strand.

This strand-biased removal of Cas9 from its DSB is interesting to consider alongside recent biochemical analyses of dCas9 dissociation from DNA. The DNA emerging from the PAM-proximal surface of Cas9 is double stranded and is not accessible to exogenous ssDNA for strand invasion (Richardson et al., 2016). Because of the RNA:DNA hybrid between the sgRNA and target DNA, the DNA emerging from the PAM-distal surface is single stranded, and ssDNA hybridization to the PAM-distal sequence can displace dCas9 from its target (Jinek et al., 2014; Nishimasu et al., 2014; Richardson et al., 2016). Mismatched base-pairing had the greatest effect on dCas9 dissociation when located at PAM-distal positions, suggesting that the 5′ end of the guide RNA contributes most significantly to the Cas9 off-rate (Boyle et al., 2017). RNAPs approaching the PAM-distal surface of the Cas9-DSB complex should have freedom to collide with Cas9. We suggest that a physical collision from RNAPs dislodges Cas9 from the DSB, facilitating repair of the DSB, and enabling the Cas9 molecule to cut an additional target DNA. The GC content of the target site and sequence adjacent to the PAM did not significantly affect displacement of Cas9 from the DSB for either orientation. Further biophysical studies are needed to determine why some template sgRNAs are more affected by Pol II translocation than others.

Multiple studies have shown that after the CRISPR-Cas9 immune response, some of the acquired viral spacers are highly represented in the population of surviving bacteria (Heler et al., 2015; Paez-Espino et al., 2013). Most likely, multiple factors determine the success of a new spacer, but it is tempting to speculate that one such factor could be the disposition of the target sequence with respect to its transcription. Our results suggest that spacers leading to the engagement of Cas9 with its target in a disposition where the nuclease can be removed by RNAP after cleavage would allow a more efficient cleavage of the often multiple phage genomes infecting the host. Such spacers would mediate a more robust immune response and therefore would be positively selected from the pool of all the acquired spacers. It is possible that the strand-biased PAM sequences of stCas9 and spCas9 evolved to target the strand of bacteriophage genomes, where it can become multi-turnover. In comparing evolution of PAM sequences and bacteriophage genomes, it should be noted that the distribution of PAM sequences on either strand of the bacteriophage genome may differ among bacteriophages that infect a given bacteria. However, in the organisms examined here (*Streptococci* and their associated bacteriophage), the PAM sequence used by Cas9 to target the more effective strand is relatively simple, and altering it requires only a small number of mutations (Kleinstiver et al., 2015). By contrast, the GC skew is pervasive over the entirety of the bacteriophage genome and is effectively unchangeable relative to the PAM sequence. We propose that targeting the bacteriophage template strand provides an advantage, because it will more frequently result in multi-turnover nucleases upon transcription of lytic genes.

STAR★METHODS

Detailed methods are provided in the online version of this paper and include the following:

- KEY RESOURCES TABLE
- CONTACT FOR REAGENT AND RESOURCE SHARING
- EXPERIMENTAL MODEL AND SUBJECT DETAILS
  - Cell culture
- METHOD DETAILS
  - Recombinant Cas9 purification
  - sgRNA synthesis for *in vitro* Cas9-RNP
  - DNA templates for *in vitro* Cas9 nuclease reactions
  - *In vitro* Cas9 DSB formation assays
  - Ku70/80 competition assay
  - Mammalian nuclear extract preparation
  - Nuclear extract and Cas9-VPR transcriptional activity validation (qPCR)
  - Fluorescent Cas9-RNP displacement assay
  - Transfection and selection conditions
  - Western blot
  - Ku70/80 Chromatin Immunoprecipitation (ChIP)
  - T7 endonuclease 1 assays
  - Flow cytometry
  - Targeted deep-sequencing preparation
  - Generation of spacers targeting ΦNM1
  - ΦNM1 infection assays
- QUANTIFICATION AND STATISTICAL ANALYSIS
  - Agarose gel quantifications
  - Targeted deep-sequencing analysis
  - Bioinformatic analysis of RNA seq versus indel frequencies
  - Agarose gel quantifications for T7E1
  - ChIP-qPCR comparisons
  - Targeted deep-sequencing comparisons
  - Bioinformatic analysis of RNA seq versus indel frequencies
- DATA AND SOFTWARE AVAILABILITY

SUPPLEMENTAL INFORMATION

Supplemental Information includes six figures and four tables and can be found with this article online at https://doi.org/10.1016/j.molcel.2018.06.005.

ACKNOWLEDGMENTS

We would like to thank Ying Su and Dr. Arnon Lavie for assistance with the purification of Cas9, Dr. Sylvain Moineau for assistance with bacteriophage genomics, Dr. Stefan Green and the DNA Services core facility at UIC for assistance with sequencing, and Dr. Miljan Simonovic for his assistance with interpretation of *in vitro* experiments. This work was supported by the NIH (grant R01-HD081534 to B.J.M. and grant 1DP2AI104556 to L.A.M.) and the UIC Center for Clinical and Translational Sciences (through NIH grant UL1TR002003 to R.C. and M.S.M.). R.H. is the recipient of a Howard Hughes International Student Research Fellowship. L.A.M. is supported by the Rita Allen Scholars Program, a Burroughs Wellcome Fund PATH award, and an HHMI-Simons Faculty Scholar Award. N.Y.C. and G.M.C. are supported by an NIH National Human Genome Research Institute grant (RM1 HG008525) and the Wyss Institute for Biologically Inspired Engineering. A.C. is supported by a Burroughs Wellcome Fund CAMS award.

AUTHOR CONTRIBUTIONS

R.C. and B.J.M. jointly designed the study. R.H. and L.A.M. conceived the phage experiments. R.C., R.H., M.S.M., and M.R. designed and performed experiments. L.H., G.M.C., and M.R. provided reagents. R.C., and M.S.M. conducted analysis of mutation frequency, with technical advice and support from N.C.Y. A.C. R.C., R.H., L.A.M., and B.J.M. wrote the manuscript with significant advice and discussion from all authors.

DECLARATION OF INTERESTS

L.A.M is the founder of Intellia Therapeutics and a member of its scientific advisory board. G.M.C.'s technology transfer, advisory roles, and funding sources are declared at arep.med.harvard.edu/gmc/tech.html. The remaining authors declare no competing interests.

Received: November 9, 2017
Revised: March 6, 2018
Accepted: June 1, 2018
Published: July 5, 2018

REFERENCES

Achigar, R., Magadán, A.H., Tremblay, D.M., Julia Pianzzola, M., and Moineau, S. (2017). Phage-host interactions in Streptococcus thermophilus: Genome analysis of phages isolated in Uruguay and ectopic spacer acquisition in CRISPR array. Sci. Rep. *7*, 43438.

Anders, C., Niewoehner, O., and Jinek, M. (2015). In vitro reconstitution and crystallization of Cas9 endonuclease bound to a guide RNA and a DNA target. Methods Enzymol. *558*, 515–537.

Barrangou, R., and Doudna, J.A. (2016). Applications of CRISPR technologies in research and beyond. Nat. Biotechnol. *34*, 933–941.

Barrangou, R., and Marraffini, L.A. (2014). CRISPR-Cas systems: prokaryotes upgrade to adaptive immunity. Mol. Cell *54*, 234–244.

Barrangou, R., Fremaux, C., Deveau, H., Richards, M., Boyaval, P., Moineau, S., Romero, D.A., and Horvath, P. (2007). CRISPR provides acquired resistance against viruses in prokaryotes. Science *315*, 1709–1712.

Boyle, E.A., Andreasson, J.O.L., Chircus, L.M., Sternberg, S.H., Wu, M.J., Guegler, C.K., Doudna, J.A., and Greenleaf, W.J. (2017). High-throughput biochemical profiling reveals sequence determinants of dCas9 off-target binding and unbinding. Proc. Natl. Acad. Sci. USA *114*, 5461–5466.

Chari, R., Mali, P., Moosburner, M., and Church, G.M. (2015). Unraveling CRISPR-Cas9 genome engineering parameters via a library-on-library approach. Nat. Methods *12*, 823–826.

Chavez, A., Scheiman, J., Vora, S., Pruitt, B.W., Tuttle, M., P R Iyer, E., Lin, S., Kiani, S., Guzman, C.D., Wiegand, D.J., et al. (2015). Highly efficient Cas9-mediated transcriptional programming. Nat. Methods *12*, 326–328.

Chavez, A., Tuttle, M., Pruitt, B.W., Ewen-Campen, B., Chari, R., Ter-Ovanesyan, D., Haque, S.J., Cecchi, R.J., Kowal, E.J.K., Buchthal, J., et al. (2016). Comparison of Cas9 activators in multiple species. Nat. Methods *13*, 563–567.

Chen, J.S., Dagdas, Y.S., Kleinstiver, B.P., Welch, M.M., Sousa, A.A., Harrington, L.B., Sternberg, S.H., Joung, J.K., Yildiz, A., and Doudna, J.A. (2017). Enhanced proofreading governs CRISPR-Cas9 targeting accuracy. Nature *550*, 407–410.

Cong, L., Ran, F.A., Cox, D., Lin, S., Barretto, R., Habib, N., Hsu, P.D., Wu, X., Jiang, W., Marraffini, L.A., and Zhang, F. (2013). Multiplex genome engineering using CRISPR/Cas systems. Science *339*, 819–823.

Deltcheva, E., Chylinski, K., Sharma, C.M., Gonzales, K., Chao, Y., Pirzada, Z.A., Eckert, M.R., Vogel, J., and Charpentier, E. (2011). CRISPR RNA maturation by trans-encoded small RNA and host factor RNase III. Nature *471*, 602–607.

Garneau, J.E., Dupuis, M.E., Villion, M., Romero, D.A., Barrangou, R., Boyaval, P., Fremaux, C., Horvath, P., Magadán, A.H., and Moineau, S. (2010). The CRISPR/Cas bacterial immune system cleaves bacteriophage and plasmid DNA. Nature *468*, 67–71.

Goldberg, G.W., Jiang, W., Bikard, D., and Marraffini, L.A. (2014). Conditional tolerance of temperate phages via transcription-dependent CRISPR-Cas targeting. Nature *514*, 633–637.

Hanakahi, L.A. (2007). 2-Step purification of the Ku DNA repair protein expressed in Escherichia coli. Protein Expr. Purif. *52*, 139–145.

Heler, R., Samai, P., Modell, J.W., Weiner, C., Goldberg, G.W., Bikard, D., and Marraffini, L.A. (2015). Cas9 specifies functional viral targets during CRISPR-Cas adaptation. Nature *519*, 199–202.

Horlbeck, M.A., Witkowsky, L.B., Guglielmi, B., Replogle, J.M., Gilbert, L.A., Villalta, J.E., Torigoe, S.E., Tjian, R., and Weissman, J.S. (2016). Nucleosomes impede Cas9 access to DNA in vivo and in vitro. eLife *5*, 5.

Hsu, P.D., Scott, D.A., Weinstein, J.A., Ran, F.A., Konermann, S., Agarwala, V., Li, Y., Fine, E.J., Wu, X., Shalem, O., et al. (2013). DNA targeting specificity of RNA-guided Cas9 nucleases. Nat. Biotechnol. *31*, 827–832.

Jin, J., Li, Z.J., Wang, S.W., Wang, S.M., Chen, S.J., Huang, D.H., Zhang, G., Li, Y.H., Wang, X.T., Wang, J., and Zhao, G.Q. (2014). Genome organisation of the Acinetobacter lytic phage ZZ1 and comparison with other T4-like Acinetobacter phages. BMC Genomics *15*, 793.

Jinek, M., Chylinski, K., Fonfara, I., Hauer, M., Doudna, J.A., and Charpentier, E. (2012). A programmable dual-RNA-guided DNA endonuclease in adaptive bacterial immunity. Science *337*, 816–821.

Jinek, M., East, A., Cheng, A., Lin, S., Ma, E., and Doudna, J. (2013). RNA-programmed genome editing in human cells. eLife *2*, e00471.

Jinek, M., Jiang, F., Taylor, D.W., Sternberg, S.H., Kaya, E., Ma, E., Anders, C., Hauer, M., Zhou, K., Lin, S., et al. (2014). Structures of Cas9 endonucleases reveal RNA-mediated conformational activation. Science *343*, 1247997.

Jones, D.L., Leroy, P., Unoson, C., Fange, D., Ćurić, V., Lawson, M.J., and Elf, J. (2017). Kinetics of dCas9 target search in *Escherichia coli*. Science *357*, 1420–1424.

Kalkan, T., and Smith, A. (2014). Mapping the route from naive pluripotency to lineage specification. Philos. Trans. R. Soc. Lond. B Biol. Sci. *369*, 20130540.

Kiani, S., Chavez, A., Tuttle, M., Hall, R.N., Chari, R., Ter-Ovanesyan, D., Qian, J., Pruitt, B.W., Beal, J., Vora, S., et al. (2015). Cas9 gRNA engineering for genome editing, activation and repression. Nat. Methods *12*, 1051–1054.

Kleinstiver, B.P., Prew, M.S., Tsai, S.Q., Topkar, V.V., Nguyen, N.T., Zheng, Z., Gonzales, A.P., Li, Z., Peterson, R.T., Yeh, J.R., et al. (2015). Engineered CRISPR-Cas9 nucleases with altered PAM specificities. Nature *523*, 481–485.

Kleinstiver, B.P., Pattanayak, V., Prew, M.S., Tsai, S.Q., Nguyen, N.T., Zheng, Z., and Joung, J.K. (2016). High-fidelity CRISPR-Cas9 nucleases with no detectable genome-wide off-target effects. Nature *529*, 490–495.

Knight, S.C., Xie, L., Deng, W., Guglielmi, B., Witkowsky, L.B., Bosanac, L., Zhang, E.T., El Beheiry, M., Masson, J.B., Dahan, M., et al. (2015). Dynamics of CRISPR-Cas9 genome interrogation in living cells. Science *350*, 823–826.

Kwan, T., Liu, J., DuBow, M., Gros, P., and Pelletier, J. (2005). The complete genomes and proteomes of 27 Staphylococcus aureus bacteriophages. Proc. Natl. Acad. Sci. USA *102*, 5174–5179.

Levin, B.R., Moineau, S., Bushman, M., and Barrangou, R. (2013). The population and evolutionary dynamics of phage and bacteria with CRISPR-mediated immunity. PLoS Genet. *9*, e1003312.

Liao, H.K., Hatanaka, F., Araoka, T., Reddy, P., Wu, M.Z., Sui, Y., Yamauchi, T., Sakurai, M., O'Keefe, D.D., Nunez-Delicado, E., et al. (2017). In vivo target gene activation via CRISPR/Cas9-mediated trans-epigenetic modulation. Cell *171*, 1495–1507.

Lobry, J.R. (1996). Asymmetric substitution patterns in the two DNA strands of bacteria. Mol. Biol. Evol. *13*, 660–665.

Mali, P., Yang, L., Esvelt, K.M., Aach, J., Guell, M., DiCarlo, J.E., Norville, J.E., and Church, G.M. (2013). RNA-guided human genome engineering via Cas9. Science *339*, 823–826.

Nishimasu, H., Ran, F.A., Hsu, P.D., Konermann, S., Shehata, S.I., Dohmae, N., Ishitani, R., Zhang, F., and Nureki, O. (2014). Crystal structure of Cas9 in complex with guide RNA and target DNA. Cell *156*, 935–949.

Paez-Espino, D., Morovic, W., Sun, C.L., Thomas, B.C., Ueda, K., Stahl, B., Barrangou, R., and Banfield, J.F. (2013). Strong bias in the bacterial CRISPR elements that confer immunity to phage. Nat. Commun. *4*, 1430.

Pinello, L., Canver, M.C., Hoban, M.D., Orkin, S.H., Kohn, D.B., Bauer, D.E., and Yuan, G.C. (2016). Analyzing CRISPR genome-editing experiments with CRISPResso. Nat. Biotechnol. *34*, 695–697.

Quinlan, A.R., and Hall, I.M. (2010). BEDTools: a flexible suite of utilities for comparing genomic features. Bioinformatics *26*, 841–842.

Richardson, C.D., Ray, G.J., DeWitt, M.A., Curie, G.L., and Corn, J.E. (2016). Enhancing homology-directed genome editing by catalytically active and inactive CRISPR-Cas9 using asymmetric donor DNA. Nat. Biotechnol. *34*, 339–344.

Shy, B.R., MacDougall, M.S., Clarke, R., and Merrill, B.J. (2016). Co-incident insertion enables high efficiency genome engineering in mouse embryonic stem cells. Nucleic Acids Res. *44*, 7997–8010.

Slaymaker, I.M., Gao, L., Zetsche, B., Scott, D.A., Yan, W.X., and Zhang, F. (2016). Rationally engineered Cas9 nucleases with improved specificity. Science *351*, 84–88.

Uchiyama, J., Rashel, M., Takemura, I., Wakiguchi, H., and Matsuzaki, S. (2008). In silico and in vivo evaluation of bacteriophage phiEF24C, a candidate for treatment of Enterococcus faecalis infections. Appl. Environ. Microbiol. *74*, 4149–4163.

Yang, S.H., Kalkan, T., Morissroe, C., Marks, H., Stunnenberg, H., Smith, A., and Sharrocks, A.D. (2014). Otx2 and Oct4 drive early enhancer activation during embryonic stem cell transition from naive pluripotency. Cell Rep. *7*, 1968–1981.

STAR★METHODS

KEY RESOURCES TABLE

REAGENT or RESOURCE	SOURCE	IDENTIFIER
Bacterial and Virus Strains		
RN4220	Kreiswirth, BN	https://doi.org/10.1038/305709a0
S. aureus RC1	This study	N/A
S. aureus RC2	This study	N/A
S. aureus RC3	This study	N/A
S. aureus RC4	This study	N/A
ΦNM1h1	This study	N/A
ΦNM1g6	Marraffini, LA	https://doi.org/10.1038/nature13637
Chemicals, Peptides, and Recombinant Proteins		
Ribonucleotide solution mix	NEB	N0466S
WT *S. pyogenes* Cas9 protein	pMJ806	https://doi.org/10.1126/science.1225829
T7 RNAP	Dr. Miljan Simonovic	N/A
Phusion DNA polymerase	NEB	M0530L
T4 DNA Ligase	NEB	M0202L
T7 Exonuclease	NEB	M0623L
T5 Exonuclease	NEB	M0363L
Human Ku70/80	Dr. Leslyn Hanakahi	https://doi.org/10.1016/j.pep.2006.10.002
Dynabeads Protein G	ThermoFisher	10004D
Dynabeads MyOne Streptavicin C1	ThermoFisher	65001
Proteinase K	Sigma-Aldrich	P2308
α-amanitin	Sigma-Aldrich	06422
Mouse ES Cell nuclear extract	This study	N/A
Superscript III	ThermoFisher	18080044
SYBR Green Supermix	Quanta	95053
Phenol:chloroform:isoamyl (25:24:1)	Sigma-Aldrich	P2069
0.1% Gelatin	Millipore	ES-006-B
Knockout DMEM	GIBCO	10829-018
L-Glutamine	GIBCO	25030-081
Pen Strep	GIBCO	15140
HEPES	Thermo Scientific	SH30237.01
MEM NEAA	GIBCO	11140
2-mercaptoethanol	GIBCO	21985-023
LIF	Millipore	ESG1106
CHIR99021	Sigma	SML1046
Trypsin-EDTA	GIBCO	25200-072
QuickExtract DNA Extraction Solution	Epicenter	BQ0901S
T7 Endonuclease I	NEB	M0302L
Anti-Ku70/80	ThermoFisher	MA1-21818
Anti-phospho-H2AX (Ser139)	Millipore	05-636
Anti-β-actin	Cell signaling	4970
Critical Commercial Assays		
TOPO TA cloning kit	Invitrogen	K4500-01
Zymo RNA Clean & Concentrator	Zymo Research	R1013

(*Continued on next page*)

Continued

REAGENT or RESOURCE	SOURCE	IDENTIFIER
Direct-zol	Zymo Research	R2051
QIAquick PCR Purification Kit	QIAGEN	28104
Deposited Data		
HEK293T genome wide SpCas9 indel dataset	Church, GM	https://doi.org/10.1038/nmeth.3473
HEK293T RNA-seq dataset	Church, GM	https://doi.org/10.1038/nmeth.3871
Mouse Genome mm10 bed file	UCSC Table Browser	https://genome.ucsc.edu/cgi-bin/hgTables?hgsid=637009305_rhfPbi0hJpHAb1sdQOAhajXOn1By&clade=mammal&org=Mouse&db=0&hgta_group=genes&hgta_track=knownGene&hgta_table=knownGene&hgta_regionType=genome&position=&hgta_outputType=bed&hgta_outFileName=hg38.bed
Human Genome hg38 bed file	UCSC Table Browser	https://genome.ucsc.edu/cgi-bin/hgTables?hgsid=637009305_rhfPbi0hJpHAb1sdQOAhajXOn1By
phage 2972	NCBI	NC_007019
phage 128	NCBI	KT717085.1
phage 73	Moineau, S	https://doi.org/10.1038/srep43438
phage 53	Moineau, S	https://doi.org/10.1038/srep43438
phage 858	NCBI	NC_010353.1
phage 5093	NCBI	NC_012753
phage 7201	NCBI	NC_002185
prophage 20617	NCBI	NC_023503
phage Sfi11	NCBI	NC_002214
phage Sfi19	NCBI	NC_000871
phage Sfi21	NCBI	NC_000872
prophage TP-778L	NCBI	NC_022776
prophage TP-J134	NCBI	NC_020197
phage NM4	Marraffini, LA	https://doi.org/10.1038/nature13637
phage NM1	Marraffini, LA	https://doi.org/10.1038/nature13637
phage A25	NCBI	NC_028697
Raw Data (unprocessed gels)	Mendeley	https://doi.org/10.17632/k3tkmh7fj4.1
Amplicon sequencing data (40 mouse genes)	NCBI	SRP148739
Experimental Models: Cell Lines		
Mouse embryonic stem cells (mESC)		
mESC harboring Rosa26::TetOn-Otx2-mCherry	Dr. Shin-His Yang	https://doi.org/10.1016/j.celrep.2014.05.037
Oligonucleotides		
See Oligonucleotides excel file for all		
Recombinant DNA		
pSpgRNA	Addgene	47018
pMJ806	Addgene	39312
pX330	Addgene	42230
Lef1::PGK-Neo	This study	N/A
Ctnnb1::EGFP	This study	N/A
pSpmCherry1	This study	N/A
pSpmCherry2	This study	N/A
pSpmCherry3	This study	N/A
pSpmCherry4	This study	N/A
pSpmCherry5	This study	N/A

(*Continued on next page*)

Continued

REAGENT or RESOURCE	SOURCE	IDENTIFIER
pSpmCherry6	This study	N/A
pSpmCherry7	This study	N/A
pSpmCherry8	This study	N/A
pSpmCherry9	This study	N/A
pSpmCherry10	This study	N/A
pSpmCherry11	This study	N/A
pSpmCherry12	This study	N/A
pSpmCherry13	This study	N/A
pSpmCherry14	This study	N/A
pSpmCherry15	This study	N/A
pSpmCherry16	This study	N/A
pSpmCherry17	This study	N/A
pSpmCherry18	This study	N/A
pSpmCherry19	This study	N/A
pSpmCherry20	This study	N/A
pSpGFP1	This study	N/A
pSpGFP2	This study	N/A
pSpGFP3	This study	N/A
pSpLef1	This study	N/A
pDB114-SpacerConstruct	Marraffini, LA	https://doi.org/10.1038/nbt.3043
pRH320-SpacerRC1	This study	N/A
pRH322-SpacerRC2	This study	N/A
pRH324-SpacerRC3	This study	N/A
pRH326-SpacerRC4	This study	N/A
Software and Algorithms		
BLAT	Kent, WJ	https://doi.org/10.1101/gr.229202
CRISPResso	Yuan, GC	https://doi.org/10.1038/nbt.3583
BedTools	Hall, IM	https://doi.org/10.1093/bioinformatics/btq033
RStudio	R	v1.0.136
ImageJ	https://imagej.nih.gov/ij/download.html	64-bit Java 1.8.0_112
FlowJo	FlowJo	v9.3.2

CONTACT FOR REAGENT AND RESOURCE SHARING

Further information and requests for reagents can be directed to, and will be fulfilled, by the corresponding author Bradley J. Merrill (merrillb@uic.edu).

EXPERIMENTAL MODEL AND SUBJECT DETAILS

Cell culture

Mouse embryonic stem (ES) cells harboring the Rex1:EGFPd2 insertion (A gift from Dr. Austin Smith) (Kalkan and Smith, 2014), or a Rosa26::TetOn-Otx2-mCherry insertion(A gift from Dr. Shen-his Yang) (Yang et al., 2014) were maintained 10cm dishes previously coated with 0.1% gelatin in Knockout DMEM media supplemented with the following: 15% KnockOut Serum Replacement, 2mM l-Glutamin, 1mM HEPES, 1 × MEM NEAA, 55 μM 2-mercaptoethanol, 100 U/ml LIF, and 3 μM CHIR99021. Cell cultures were routinely split 1:10 with 0.25% trypsin–EDTA every 2–3 days.

HEK293 cells (A gift from Dr. Sojin Shikano) were cultured in high glucose DMEM supplemented with 10% FBS and 1% Pen/Strep and were split every 2-3 days using 0.25% trypsin–EDTA.

METHOD DETAILS

Recombinant Cas9 purification

Cas9 (pMJ806, Addgene #39312) was expressed and purified by a combination of affinity, ion exchange and size exclusion chromatographic steps as previously described (Anders et al., 2015).

sgRNA synthesis for *in vitro* Cas9-RNP

All sgRNAs were cloned into pSPgRNA (Addgene, #47108) following the protocol optimized for pX330 base plasmids (https://www.addgene.org/crispr/zhang/) (Cong et al., 2013). sgRNA oligo sequences, listed without BbsI sticky ends used for cloning, can be found in Figures S1H, S2A, and S5D. Templates for *in vitro* transcription were generated via PCR mediated fusion of the T7 RNAP promoter to the 5′ end of the sgRNA sequence using the appropriate pSPgRNA as the reaction template DNA. PCR reactions were performed using Phusion high GC buffer (NEB) and standard PCR conditions (98°C for 30 s, 30 cycles of 98°C for 5 s, 64°C for 10 s and 72°C for 15 s, and one cycle of 72°C for 5 m). PCR products were then column purified (QIAGEN) and eluted in TE (10mM Tris-HCl pH 8.0, 1mM EDTA). DNA concentrations were determined using a Nanodrop 2000 (ThermoFisher Scientific), and then were diluted to 200nM when used as templates for *in vitro* transcription reactions. The transcription reactions contained 5.0 μg/ml purified recombinant T7 RNAP (a gift from Dr. Miljan Simonovic) and 1x transcription buffer (40mM Tris-HCl pH8.0, 2mM spermidine, 10mM MgCl2, 5mM DTT, 2.5mM rNTPs). Following incubation at 37°C for 1 hour, reactions were treated with RNase free DNase I (ThermoFisher Scientific) and column purified using the Zymo RNA Clean & Concentrator kit following the manufacturer's protocol. The purified RNA products were eluted from the column in 15 μL of water.

DNA templates for *in vitro* Cas9 nuclease reactions

Linear target DNAs for hybrid digestion and transcription assays: mouse Lef1, mCherry, and GFP target DNAs were generated by PCR amplification using 50ng genomic DNA from mESC Rosa26::TetON-Otx2-mCherry cells in a reaction using Phusion high GC buffer (NEB) and standard PCR conditions (98°C for 30 s, 30 cycles of 98°C for 5 s, 64°C for 10 s and 72°C for 15 s, and one cycle of 72°C for 5 m). ΦNM1 genomic DNA was amplified with the same parameters, except using Phusion HF buffer. All PCR products were column purified (QIAGEN), eluted in TE, and concentrations were determined with a Nanodrop 2000 (ThermoFisher Scientific). For experiments testing effects of T7 RNAP on Cas9, the DNA template was a segment of the mouse Lef1 gene generated with primer set #1 (Table S4), unless otherwise stated.

Plasmid target DNAs: For reactions that required circular dsDNA templates (experiments testing accessibility of exonuclease or ligase enzymes), plasmid target DNAs were prepared using TOPO TA cloning. PCR products of the previously described Lef1::PGK-neo and Ctnnb1::EGFP DNA sequences (Shy et al., 2016) were cloned into the pCR4-TOPO Vector (ThermoFisher Scientific).

In vitro Cas9 DSB formation assays

The basic Cas9 DSB formation assay was prepared in 1x Cas9 digestion buffer (40mM Tris, pH8.0, 10mM MgCl2, 5mM DTT) with a final concentration of 100nM Cas9, unless otherwise stated. Prior to addition of DNA templates, sgRNA was added in molar excess, and incubated at room temperature for 10 min to ensure formation of the Cas9-RNP. Target DNA was added to a final concentration of 200nM and a final reaction volume of 50 μl, unless otherwise stated. Reactions were incubated at 37°C for 25 min, then either heat inactivated at 75°C for 10 min or treated with Proteinase K at 37°C for 15 min. DNA fragments from portion of each reaction (usually 15 μl) were separated by electrophoresis 1.5% agarose gel, and visualized with ethidium bromide staining.

For reactions involving T7 RNAP transcription, basic Cas9 digestion conditions were applied, except 1x transcription buffer was used, unless otherwise stated. Upon addition of the target DNA, T7 RNAP was added to a final concentration of 5.0 μg/ml. Reactions were placed at 37°C for 25 min, unless otherwise stated, and then heat inactivated at 75°C for 10 min. DNase free RNase A (NEB) was added to all reactions except Figures S4A and S5E, then incubated at 37°C for 30 min before separating DNA fragments on a 1.5% agarose gel.

T7 and T5 exonuclease assays were performed in 1x Cas9 digestion buffer, unless otherwise stated. T7 exonuclease assays was performed with the Lef1::PGK-Neo plasmid and digested using sgLef1. T5 exonuclease assays were performed with Ctnnb1::EGFP plasmid and digested using sgG2. T5 exonuclease assays containing T7 RNAP were performed in 1x transcription buffer. All reactions contained 100nM Cas9:RNP, 200nM target DNA, and 10U of the appropriate exonuclease. Reactions were subject to Proteinase K treatment before loading onto a 1% agarose gel.

T4 DNA ligase and Cas9 digestion assays were performed in T4 DNA Ligase buffer containing ATP (NEB). Cas9 containing reactions were performed with 200nM Cas9:RNP (sgLef1) and 100nM Lef1::PGK-Neo plasmid were allowed to incubate for 30 min at 37°C, then the temperature was lowered to 16°C and 40U of T4 DNA ligase (NEB) was added and allowed 30 min of incubation. Reactions were transformed into competent DH5a in 3 serial dilutions, and ampicillin-resistant colony forming units determined following overnight incubation at 37°C.

Titrations of Cas9 or substrate: Cas9 hybrid digestion and transcription reactions were performed using sgG2 and a GFP target DNA generated with primer set #6 (Table S4). Cleavage frequencies were measure using ImageJ.

Ku70/80 competition assay

Recombinant human Ku70/80 was purified as previously described (Hanakahi, 2007). A 5′ biotinylated primer (5′ *BIOSG*-GCCTCACACGGAATCT 3′) and a 3′ FAM conjugated primer (5′ GAGAGCCCTCTCCCAATCTTC-*FAM* 3′) (Integrated DNA Technologies) were used to amplify a 650bp Lef1 target DNA, PCR products were column purified (QIAGEN), and eluted in TE. MyOne Dynabeads (ThermoFisher) were prepared as described by the manufacturer to immobilize 750ng of target DNA to ~4 μL of beads. Cas9 and sgRNA were pre-incubated in 1x Cas9 digestion buffer (40mM Tris, pH8.0, 10mM MgCl2, 5mM DTT) for 30 min at room temperature, added to the immobilized DNA in a 5:1 molar ratio, and incubated for 25 min at 37°C. Control reactions without Cas9, but containing DNase, NcoI, and/or Ku70/80 were prepared simultaneously and incubated for 25 min at 37°C. Reactions containing Cas9 were then subject to Proteinase K treatment or addition of excess Ku70/80 (100 fold excess), and incubated for 15 min at 37°C. Bead-bound DNA fragments were then collected by placing reaction tubes on a magnet, and 10 μL of the soluble fraction was transferred to a 384 well plate in technical triplicates. FAM fluorescence levels were measured using a Tecan Infinite Pro200. Calculations were made after subtracting the background fluorescence levels of reactions containing the immobilized but uncleaved FAM labeled DNA. Three independently set up reactions were performed for each reaction condition.

Mammalian nuclear extract preparation

mESC were grown in a 10cm dish to $10x10^6$ confluency and scraped into 3 mL PBS, then pelleted at 16,000 rpm for 10 min at 4°C. The supernatant was then aspirated and the pellet was resuspended in 800 ul of ice cold Buffer A (10mM HEPES pH 7.9, 1.5mM MgCl2, 10mM KCL, 0.5mM DTT, and 1% protease inhibitors). The pellet was incubated on ice for 10 min, vortexed for 10 s, then centrifuged at 4°C at 4,000 rpm for 10 min. The supernatant (cytoplasmic fraction) was discarded, and the pellet was resuspended in 200 μL of Buffer B (10mM HEPES pH 7.9, 0.4mM NaCl, 10mM KCL, 1.5mM MgCl2, 0.1mM EDTA, 12.5% glycerol, 0.5mM DTT, and 1% protease inhibitors). The resuspended pellet was incubated on ice for 30 min then centrifuged at 14,000 rpm for 20 min at 4°C. The supernatant (nuclear fraction) was aliquoted and stored at −80°C.

Nuclear extract and Cas9-VPR transcriptional activity validation (qPCR)

Nuclear extracts: nuclear extract (6 μL per reaction) was added to reactions containing: 12 μL 1x NE transcription buffer (20mM HEPES pH 7.9, 100mM KCL, 0.2mM EDTA, 0.5mM DTT, 20% glycerol), 3 μL of 50mM MgCl2, 1.2 μL 25mM rNTPs, and 38nM CMV-mCherry (serving as Pol II transcription template, see below for PCR amplification procedure) to create final reaction volumes of 45 μl. Control reactions contained 6 μg of α-amanitin (Sigma-Aldrich #04622) or lacked rNTPs. Reactions were incubated at 37°C for 45 min, then 10U of DNase I was added (ThermoFisher) and incubated at 37°C for 30 min. After completion of DNA digestion, 150 μL of TE and 200 μL of 25:24:1 phenol:chloroform:isoamyl (Sigma-Aldrich) were added. Reactions were then vortexed for 15 s, briefly centrifuged, then the aqueous layer was transferred to a fresh 1.5 mL tube. RNA was precipitated from the mixture by adding 3 volumes of ice cold 100% ethanol, then centrifuged for 10min at top speed. RNAs were reconstituted in water and diluted to 500ng/μl. 1 μg of RNA was converted to cDNA using Superscript III (ThermoFisher) and quantitative real time PCR was performed using primer set #10 (Table S4) by combining 250ng of cDNA from each sample was with Perfecta SYBR Green Supermix (Quanta #95053). qPCR was performed on a C1000 thermal cycler and CFX96 Real Time System (Bio-Rad) with the following parameters: 95°C for 2 min, then 40 cycles of 95°C for 30 s and 60°C for 45 s. Quantities were normalized to control reactions of CMV-mCherry DNA used to create a standard curve. Standard log transformation of Ct values and standard curve equation was then applied before calculating fold change of experimental conditions over the no rNTP condition.

Cas9-VPR transcriptional activation validation: 48 hours after transfection of reagents containing Cas9-VPR targeted to TTN with a 14nt sgRNA, roughly 1.5 million HEK293 cells were harvested for RNA through washing twice with PBS then adding 600ul of Trizol. RNA was purified using the DirectZol kit (Zymo) including the DNase I digestion step. Purified RNA was eluted using 20ul of water. cDNA generation and qPCR protocol was performed as mentioned above. Transcriptional activity of Cas9-VPR at the target site was analyzed through calculating ΔΔCt for the sgTTN (correctly targeted) condition to a non-targeted control.

Fluorescent Cas9-RNP displacement assay

Generation of Pol II or T7 RNAP promoter containing target DNAs: CMV-mCherry was amplified with primer set #11 (Table S4) to include the polyA from pmCherry-C1 (Clontech), and T7-mCherry was amplified with primer set #4 (Table S4). PCRs conditions contained Phusion high HF buffer (NEB) and standard PCR conditions (98°C for 30 s, 30 cycles of 98°C for 5 s, 64°C for 10 s and 72°C for 20 s, and one cycle of 72°C for 5 m), and PCR products were column purified (QIAGEN), and eluted in TE.

Generation of displaced Cas9 fluorescent detection substrates: Fluorescent target DNAs (FT-DNA) were generated to contain 3 or 4 Cas9 target sites per FT-DNA to accommodate all 20 mCherry sgRNA, rendering DNAs that range from 134bp to 90bp (Table S2). FT-DNAs were prepared by ordering single stranded sense ultramers (IDT) and PCR amplifying with a 5′ biotinylated primer (5′ *BIOSG*-CGTAAACGGCCACAAGTTCAG 3′) and a 3′ FAM conjugated primer (5′ CTTGTACAGCTCGTCCATGCC-*FAM* 3′). PCR conditions consisted of Phusion high HF buffer (NEB) and standard PCR conditions (98°C for 30 s, 30 cycles of 98°C for 5 s, 61°C for 10 s and 72°C for 5 s, and one cycle of 72°C for 5 m), and PCR products were column purified (QIAGEN), and eluted in TE.

Displacement assays with mammalian nuclear extracts: To test the effect of Pol II, Cas9 digestion reactions were carried out in 15 μL reactions containing: in 4 μL of 1x NE transcription buffer, 1 μL of 50mM MgCl2, 0.4 μL 25mM rNTPs, and 2.1 μL of freshly thawed nuclear extract. Cas9 was added to a final concentration of 26nM and respective sgRNA was added in excess, then

incubated at RT for 10 min to allow formation of RNP. After formation of the RNP, 6 μg of α-amanitin was added to respective reactions, then CMV-mCherry was added to a final concentration to all reactions to a final concentration of 38nM and to render a final volume of 15ul for all reactions. Reactions were then incubated at 37°C for 45 min. While the hybrid transcription/digestion reactions were incubating, FT-DNAs were immobilized to MyOne Dynabeads (ThermoFisher) as described by the manufacturer. The immobilized FT-DNAs were heated at 75°C for 5 min to remove non-specific binding, then washed twice, then resuspended in 1x NE transcription so FT-DNA was at a concentration of 100ng/μl. Upon completion of the Cas9 transcription/digestion reactions, the bead:FT-DNA conjugates were added to each reaction so FT-DNAs were in 2:1 molar ratio to CMV-mCherry. The reactions were incubated at 37°C for 15min, then heated at 75°C for 10 min to denature the displaced Cas9 which was bound to FT-DNAs thereby releasing the cleaved fluorescent end of the FT-DNAs into the soluble fraction. All reactions were then placed on a magnet, and the soluble fraction was removed and placed into a suitable plate for reading FAM fluorescence levels were measured using a Tecan Infinite Pro200. Calculations were made after subtracting the background fluorescence levels of reactions containing the immobilized but uncleaved FT-DNAs respectively. Two independently set up reactions were performed for each reaction condition.

Displacement assays with T7 RNAP: Reactions were performed in the exact manner as the mammalian nuclear extract displacement assays except with minimal changes: reaction buffer was 1x transcription buffer, and presence or absence of transcription was controlled through presence or absence of rNTPs rather than using α-amanitin. Two independently set up reactions were performed for each reaction condition.

Transfection and selection conditions

Within 2 hr of transfections, 0.25 × 10^5 ES cells were freshly plated in each well of 24 wells dishes. For each well, 2.5 μL of Lipofectamine 2000 and relevant DNAs were incubated in 125 μL OPTI-MEM (GIBCO #31985) before adding to wells. For the Cas9 mutagenesis of 40 distinct genes in ES cells, transfections included 150ng pPGKpuro (Addgene plasmid # 11349), 150ng pX330 (lacking sgRNA insert), and 150ng of the relevant pSPgRNA plasmid. To assess background mutation rate due to possible deep sequencing or amplification errors, a transfection containing pSPgRNA with empty sgRNA site was assessed alongside the other sgRNA-containing transfections. Two days after transfection, cells were split into 2 μg/ml puromycin and selection was applied for 48hrs before isolating genomic DNA by overnight lysis with Bradley Lysis buffer (10mM Tris-HCl, 10mM EDTA, 0.5% SDS, 10mM NaCl) containing 1mg/ml Proteinase K, followed with EtOH/NaCl precipitation, two 70% EtOH washes, and eluted in 50 μL of TE. For mCherry targeting, transfections contained the same DNA, except pSPgRNA targeted the mCherry genomic insertion, genomic DNA was isolated 48 hours after transfection in 50 μL of Quick Extract solution (Epicenter) for T7E1 assays.

Western blot

~2 million ES cells were collected from 6 well plates after washing twice with PBS, then scraping into 600ul of PBS followed by pelleting at 5,000 rpm for 5 minutes. The cell pellet was then resuspended in 100ul of pre-heated (98°C) 2x Laemmli lysis buffer (4% SDS, 20% glycerol, 120mM Tris-Cl, 0.02% w/v bromophenol blue) and heated at 98°C for 10 m. While still hot, each sample was resuspended with a 25 gauge needle to shear genomic DNA. 25μl of each sample was loaded onto a 12% SDS-PAGE gel and then transferred to 0.22μm PVDF membranes. Membranes were blocked for 1 hour at room temperature with 5% BSA before probing for phospho-H2AX, or 5% milk before probing for β-actin. Anti-phospho-H2AX was diluted to 0.05ug/ml in 5% BSA, and anti-β-actin was diluted 1:2000 in 5% milk. Both primary antibodies were incubated o/n at 4°C.

Ku70/80 Chromatin Immunoprecipitation (ChIP)

~3.5 million ES cell were seeded onto 10cm dishes in 9ml of media then immediately transfected with a 1ml solution containing Cas9 expression and 4 template or 4 non-template sgRNA expression plasmids. 24 hours after transfection, crosslinking was performed by adding 270 μL of 37% formaldehyde to each dish. Cells were then rotated gently at RT for 12.5 min, and then 540 μL of 2.5M glycine was added to quench the reaction. Cells were then washed with cold phosphate buffered saline (PBS) twice prior to harvesting by silicon cell scrapers and centrifugation (4°C, 4000 rpm), followed by flash freezing with liquid nitrogen and storage at −80°C. After thawing, all subsequent steps were performed at 4°C or on ice and fresh protease inhibitors were added to each lysis buffer. Cells were resuspended in lysis buffer (LB) 1 (50 mM HEPES pH 7.7, 140 mM NaCl, 1 mM EDTA, 10% Glycerol, 0.5% NP-40, 0.25% Trtiton-X-100) and gently rotated for 20 min. Cells were pelleted for 10 min at 2500 RPM and then in LB 2 (200 mM NaCl, 1 mM EDTA, 0.5 mM EGTA, 10 mM Tris pH 7.5). After incubation for 10 minutes under constant rotation, cells were pelleted again and resuspended in LB 3 (1 mM EDTA, 0.5 mM EGTA, 10 mM Tris pH 7.5, 100 mM NaCl, 0.1% Na-deoxycholate). Sonication was performed using a Branson Digital Sonifier 450 at 60% amplitude on ice for 15 cycles (30 s ON, 60 s OFF) to obtain an average DNA fragment size of 500 bp. After sonication, 1/10 volume of 10% Triton X-100 was added and then the samples were centrifuged for 10 min at max speed to remove cellular debris. 100 μL of each chromatin extract was uncrosslinked at 65°C overnight, treated with RNaseA for 1 hour, then proteinase K for 1 hour, and then purified using phenol/chloroform extraction and ethanol precipitation to determine the concentration of DNA and to serve as an input control.

To prepare the Ku70/80 antibody for immunoprecipitation, 4ug antibody per ChIP was incubated with 20ul of Protein G Dynabeads. Each condition was split into three technical triplicates and then Ku70/80 immunoprecipitation was performed by incubating 10 μg chromatin extract overnight at 4°C with the antibody bound beads while gently rocking. The beads were then washed 4 times with 500ul RIPA buffer (50 mM HEPES, 1mM EDTA, 0.7% Na-deoxycholate, 1% NP-40, 0.5 M LiCl) and once with 500ul TBS

(50 mM Tris, 150 mM NaCl, pH 7.6). Bound complexes were eluted from the beads by resuspending in 400ul elution buffer (50mM Tris pH 8, 10mM EDTA, 1% SDS) and heating at 65°C with occasional vortexing. Crosslinks were reversed by incubation at 65°C overnight, and samples were treated with RNase A and proteinase K subsequently for 1 hour each. DNA was isolated using phenol-chloroform extraction and ethanol precipitation, followed by resuspension in 200ul Tris-EDTA. To compare the amount of immunoprecipitated DNA for each condition, qPCR was performed following the aforementioned general protocol. 5ul input and ChIP DNA for each condition was added to each 25ul qPCR reaction, and Gapdh served as the negative control region. Primers used for quantitative PCR following ChIP are listed in the Table S4. Ct values for each input were corrected to account for the difference in starting chromatin extract amount for input versus ChIP, and then the level of DNA immunoprecipitated as detected by the qPCR was calculated as a % of input for each condition. Finally, the % input of each target site was divided by the % input of the Gadph control to determine fold enrichment of Ku70/80 bound DNA.

T7 endonuclease 1 assays

Genomic DNA was used as a template in a PCR reaction using Phusion polymerase (NEB) and standard PCR conditions (98°C for 30 s, 30 cycles of 98°C for 5 s, 55°C for 10 s and 72°C for 25 s, and one cycle of 72°C for 5 m). 5 μL of each PCR product was added to 19 μL of 1x NEBuffer 2 (NEB), denatured at 95C for 10 min, then brought down to room temperature by decreasing the temperature 1C per second. 1 μL of T7E1 (NEB) was added to each reaction, and allowed to incubate at 37°C for 25 min. DNA fragments were separated by electrophoresis through a 1.5% agarose gel. Gel images were analyzed and indel frequencies were quantified using ImageJ.

Flow cytometry

Single-cell suspensions were prepared by trypsinization and re-suspension in 2% FBS/PBS/2mM EDTA. Cells were analyzed on a LSRFortessa flow cytometer. Data analysis was performed using FlowJo v9.3.2. Live cells were gated by forward scatter and side scatter area. Singlets were gated by side scatter area and side scatter width. At least 5×10^5 singlet, live cells were counted for each sample. mCherry fluorescence events were quantified by gating the appropriate channel using fluorescence negative cells as control.

Targeted deep-sequencing preparation

Preparation: genomic DNA was harvested four days after transfection and approximately 100ng of DNA was used in PCR to amplify respective target sites while attaching adaptor sequences for subsequent barcoding steps (Table S1 for NGS primers). PCR products were analyzed via agarose gel and then distinct amplicons were pooled for each replicate respectively in equal amounts based on ImageJ quantification. Pooled PCR products were purified with AMPure beads (Agilent), and 5ng of the purified pools was barcoded with Fluidigm Access Array barcodes using AccuPrimer II (ThermoFisher Scientific) PCR mix (95°C for 5 m, 8 cycles of 95°C for 30 s, 60°C for 30 s and 72°C for 30 s, and one cycle of 72°C for 7 m). Barcoded PCR products were analyzed on a 2200 TapeStation (Agilent) before and after 2 rounds of 0.6x SPRI bead purification to exclude primer dimers. A final pool of amplicons was created and loaded onto an Illumina MiniSeq generating 150bp paired-end reads.

Generation of spacers targeting ΦNM1

Plasmids harboring Cas9, tracrRNA and single-spacer arrays targeting ΦNM1 were constructed via BsaI cloning onto pDB114 as described previously (Heler et al., 2015). Specifically, spacers RC1 (plasmid pRH320), RC2 (pRH322), RC3 (pRH324) and RC4 (pRH326) were constructed by annealing oligo pairs H560-H561, H564-H565, H568-H569 and H572-H573, respectively. Each pair of annealed oligos contains compatible BsaI overhangs and can be found in Table S3.

ΦNM1 infection assays

Phage ΦNM1h1 was isolated as an escaper of CRISPR type III targeting of ΦNM1 with spacer 4B (Goldberg et al., 2014). Plate reader growth curves of bacteria infected with phage were conducted as described previously (Goldberg et al., 2014) with minor modifications. Overnight cultures were diluted 1:100 into 2ml of fresh BHI supplemented with appropriate antibiotics and 5mM CaCl2 and grown to an OD600 of ~0.2. Immune cells carrying targeting spacers were diluted with cells lacking CRISPR-Cas in a 1:10,000 ratio and infected with either ΦNM1h1 or ΦNM1g6 at MOI 1. To produce plate reader growth curves, 200 μL of infected cultures, normalized for OD600, were transferred to a 96-well plate in triplicate. OD600 measurements were collected every 10 min for 24 hr.

QUANTIFICATION AND STATISTICAL ANALYSIS

Agarose gel quantifications

For all Cas9 digestion reactions and T7E1 assays, percent cleavage values were determined by measuring densitometry of individual DNA bands in ImageJ, then dividing the total cleaved DNA by total DNA.

Targeted deep-sequencing analysis

Determination of indel frequencies made use of CRISPResso command line tools that demultiplexed by amplicon, where appropriate, and then determined indel frequency by alignment to reference amplicon files (Pinello et al., 2016). Outputs were assembled and analyzed using custom command-line, python, and R scripts which are available upon request.

Bioinformatic analysis of RNA seq versus indel frequencies

The source of large scale indel mutagenesis and RNA-seq data were from previously published reports (Chari et al., 2015; Chavez et al., 2016). Blat and bedtools command line tools (Quinlan and Hall, 2010) were used to classify each of the sgRNA used by Chari et al. (Chari et al., 2015) as targeting either the template or non-template gene strand. All data were merged and visualized using RStudio version 1.0.136 (package: ggplot2), allowing for the determination of the effect of FPKM and strand orientation on indel frequency.

Agarose gel quantifications for T7E1

The three biological replicates of the mutagenesis data presented in Figure 1E were analyzed for statistical significance using RStudio. Statistical analyses were performed by generating p values for each sgRNA with a two sample t test to compare plus and minus doxycycline, then all p values were adjusted via Bonferroni correction.

ChIP-qPCR comparisons

Template and non-template groups for each gene were analyzed for statistical significance in R studio using a two sample t test where all p values were adjusted via Bonferroni correction

Targeted deep-sequencing comparisons

Statistical analyses were performed by pooling indel frequencies for all sgRNA annealing to the template or non-template strand, creating two separate groups. Then, unpaired, two tailed t test was performed.

Bioinformatic analysis of RNA seq versus indel frequencies

Statistical analyses and significance were determined with Multiple Comparisons of Means with Tukey contrasts (package: multcomp).

DATA AND SOFTWARE AVAILABILITY

All scripts for statistical analysis or preparation of NGS data mentioned throughout the methods section are available upon request.

Raw sequencing data will be available on NCBI (SRP148739). Unprocessed gels are available on Mendeley (https://doi.org/10.17632/k3tkmh7fj4.1).